Paleoceanography and Paleoclimatology

RESEARCH ARTICLE
10.1029/2019PA003827

Key Points:
- Benthic-planktic coupling and its response to past suborbital climate variability
- Carbon export and hydrology mainly drive benthic changes before 6 ka
- Dry/humid climate oscillations affect the nature of primary producers and the response of foraminiferal species after 6 ka

Supporting Information:
- Supporting Information S1

Correspondence to:
S. Le Houedec,
sandrine.lehouedec@univ-angers.fr

Citation:
Le Houedec, S., Mojtahid, M., Bicchi, E., de Lange, G. J., & Hennekam, R. (2020). Suborbital hydrological variability inferred from coupled benthic and planktic foraminiferal-based proxies in the southeastern Mediterranean during the last 19 ka. *Paleoceanography and Paleoclimatology*, *35*, e2019PA003827. https://doi.org/10.1029/2019PA003827

Received 18 DEC 2019
Accepted 11 FEB 2020
Accepted article online 13 FEB 2020

Suborbital Hydrological Variability Inferred From Coupled Benthic and Planktic Foraminiferal-Based Proxies in the Southeastern Mediterranean During the Last 19 ka

S. Le Houedec[1], M. Mojtahid[1], E. Bicchi[1,2], G. J. de Lange[3], and R. Hennekam[4]

[1]LPG-BIAF UMR-CNRS 6112, UNIV Angers, UNIV Nantes, CNRS, Angers, France, [2]Esaip La Salle, Cerade, St-Barthélemy d'Anjou, France, [3]Department of Earth Sciences-Geochemistry, Faculty of Geosciences, Utrecht University, Utrecht, The Netherlands, [4]Department of Ocean Systems, NIOZ Royal Netherlands Institute for Sea Research and Utrecht University, Texel, The Netherlands

Abstract We present a high-resolution study covering the past 19 ka from the southeastern Mediterranean Sea, based on benthic foraminiferal faunas and their stable oxygen and carbon isotopes. These data are integrated with previously published and newly acquired planktic foraminiferal data from the same sediment core in order to investigate the benthic-planktic coupling and its response to past suborbital climate variability. On a millennial timescale, foraminiferal communities and their isotopic signatures vary following three main time periods (late glacial, sapropel S1 [~10.1–6.5 ka], and mid-Holocene to Late Holocene). Within these intervals, we identified short-timescale changes related to the carbon export and hydrological conditions. During the deglaciation, and except for the Younger Dryas, the coupled benthic-planktic data indicate an overall poorly mixed water column with a low productivity. During S1 event, our data confirm the presence of a highly stratified water column, with enhanced primary productivity export to the deep sea, being associated to high Nile River activity. While the foraminiferal ecosystem is strongly driven by the combined influence of overturning circulation and the Nile River activity until the end of the African humid period, we suggest a more regional eastern Mediterranean climatic-driven response of the foraminiferal community over the mid-Holocene to Late Holocene. A strong multicentennial variability, probably associated to solar forcing, was found for both benthic and planktic records, and a supplementary 1,600-year mode was found for the benthic data, suggesting a potential overturning circulation-driven forcing for the latter.

1. Introduction

Understanding climate dynamics and its effect on ecosystem functioning remains a challenge of increasing relevance in our modern era of CO_2-driven climate change. The Mediterranean region was identified as one of the major climatic hot spots (Giorgi, 2006; Hoegh-Guldberg et al., 2018; Turco et al., 2015). Numerous climate models concordantly point to a warmer and drier future climate for this region, particularly for the eastern Mediterranean region (Adloff et al., 2015; Giorgi & Lionello, 2008; Li et al., 2012). Still, studying past environmental variability and ecosystem functioning in this region is of pivotal importance to (i) expose associated climatic forcing factors and processes involved and (ii) better constrain the consequences of such a warmer and drier future on these marine ecosystems. The Late Quaternary climate and environmental variability has already been assessed in this region in numerous marine and terrestrial studies (e.g., Almogi-Labin et al., 2009; Bar-Matthews et al., 1997, 1999; Bartov et al., 2003; Castañeda et al., 2010; deMenocal, Ortiz, Guilderson, Adkins, et al., 2000; Dormoy et al., 2009; Ehrmann et al., 2007; Essallami et al., 2007; Gasse et al., 2011; Giamali et al., 2019; Kontakiotis, 2016; Kotthoff et al., 2008; Revel et al., 2014), allowing to identify several contrasting key climatic periods such as the Last Glacial Maximum (LGM; ending at ~19 ka), Heinrich event 1 (H1; ~18.2–14.8 ka), the Bølling-Allerød (B/A; 14.7–12.8 ka), the Younger Dryas (YD; ~12.8–11.5 ka), the African humid period (AHP, ~11–5 ka) including sapropel S1 (~10.1–6.5 ka) and its two phases S1a (~10.1–8.2 ka) and S1b (~7.9–6.5 ka; Hennekam et al., 2014), the Roman Warm Period (RWP; ~2.6–1.6 ka), the Medieval Warm Period (MWP; 1.1–0.54 ka), and the Little

Ice Age (0.54–0.1 ka). However, it remains elusive how these climatic intervals, which affect surface water conditions, impact the deeper part of the Mediterranean Sea. In the eastern Mediterranean (EM), some studies focused on the deep-sea benthic ecosystems and demonstrated that they are able to record changes in the North Atlantic oceanic circulation and the regional dynamics controlling bottom water oxygenation and food availability (e.g., Abu-Zied et al., 2008; Giunta et al., 2003; Jorissen, 1999; Kuhnt et al., 2007; Schmiedl et al., 2003, 2010, Louvari et al., 2019). Other studies focused on coupled benthic and planktic $\delta^{13}C$ signatures and/or model experiments to address the impact of past climatic changes in the EM (Grimm et al., 2015; Schilman, Almogi-Labin, et al., 2001, 2003). In this study, we couple high time-resolution surface and bottom foraminiferal data (species composition and stable oxygen and carbon isotopes) from the same sedimentary record covering the past 19 ka. This paired benthic-planktic approach, coupling ecology and isotopy, is unique in terms of time coverage in the EM and is advantageous to fully understand sea surface to deep-sea connectivity and its relation to climatic conditions.

The Levantine area is known to sensitively respond to orbital- and suborbital-induced climate variability from both the high northern latitudes and the low-latitude African/Indian monsoon systems (Almogi-Labin et al., 2009; Bar-Matthews et al., 1997, 2003; Hennekam et al., 2014; Mojtahid et al., 2015, 2019; Revel et al., 2014; Schmiedl et al., 2010). For instance, the strong imprint of H1 and YD in the EM geological archives is one of the most robust evidence for the climate of this region being related to the millennial climate variability associated to the North Atlantic (Cacho et al., 1999, 2001; Rohling et al., 1998). In contrast, the organic-rich sapropel deposits, such as the most recent sapropel S1, result from periods of enhanced northeast African monsoon system increasing the discharge from the Nile River and other North African river systems (e.g., Rohling, Cane, et al., 2002). By increasing the freshwater supply to the Levantine Basin, a strong water column stratification occurred, ceasing the ventilation of the deep sea by oxygenated waters (e.g., Grimm et al., 2015). This in turn resulted in water column deoxygenation by ongoing respiration of settling organic matter, which may have been enhanced as well by an increased nutrient input stimulating primary productivity (De Lange et al., 2008; Kallel et al., 1997; Rohling, 1994; Rossignol-Strick et al., 1982). Even though millennial timescales are well studied in the EM, we here investigate benthic-planktic coupling with a focus on shorter <1-ka timescales by using a strategically located sedimentological archive.

The present study focuses on the marine sediment core PS009PC located in the southeastern Levantine Basin and covering the past 19 ka (Figure 1). The vicinity to the Nile River and the high sedimentation rate (30 cm/ka on average) make this a suitable location to sensitively record climatically induced Nile River hydrological activity with relatively high time resolution (Hennekam et al., 2015; Revel et al., 2014). Core PS009PC was earlier studied for its inorganic geochemical properties, the oxygen composition of the planktic foraminifera *Globigerinoides ruber* (white, sensu stricto) until 13 ka (Hennekam et al., 2014; Hennekam & de Lange, 2012), planktic assemblages (Mojtahid et al., 2015), and foraminiferal elemental/calcium ratios during S1 (Mojtahid et al., 2019). In this study, we present new benthic foraminiferal faunal assemblages and stable isotope ($\delta^{18}O$ and $\delta^{13}C$) records, and we extended the planktic isotopic record with new data from 19 to 13 ka. The main scientific questions addressed in this manuscript are (i) how the benthic foraminiferal community responds to organic matter flux changes during the Late Quaternary; (ii) how the benthic-planktic coupling approach informs us about changes in the overturning circulation versus the Nile River activity; and (iii) what are the forcing processes controlling the reconstructed environmental changes.

2. Study Area

2.1. Sampling Site

Piston core PS009PC (32°07.7′N, 34°24.4′E; 552-m water depth, Figure 1) was sampled during the PASSAP cruise with the R/V Pelagia in May 2000. The core is located in the southeastern Mediterranean Sea (i.e., the Levantine Basin). The fine-grained sediments composing the studied core (i.e., >90% of clay and silt; Hennekam & de Lange, 2012), before the commissioning of the Aswan Dam, are mainly sourced from the Nile River (Krom et al., 1999). The large influence of Nile River discharge results in high sedimentation rates in this region, particularly throughout the Holocene (Almogi-Labin et al., 2009; Box et al., 2011; Castañeda et al., 2010; Hamann et al., 2009; Hennekam et al., 2015; Schilman, Bar-Matthews, et al., 2001; van Helmond et al., 2015). In our study core, the sedimentation rate is constant from 16 ka to the mid-Holocene (12 cm/ka) and increases during the Late Holocene from 12 to 100 cm/ka (Hennekam et al., 2014).

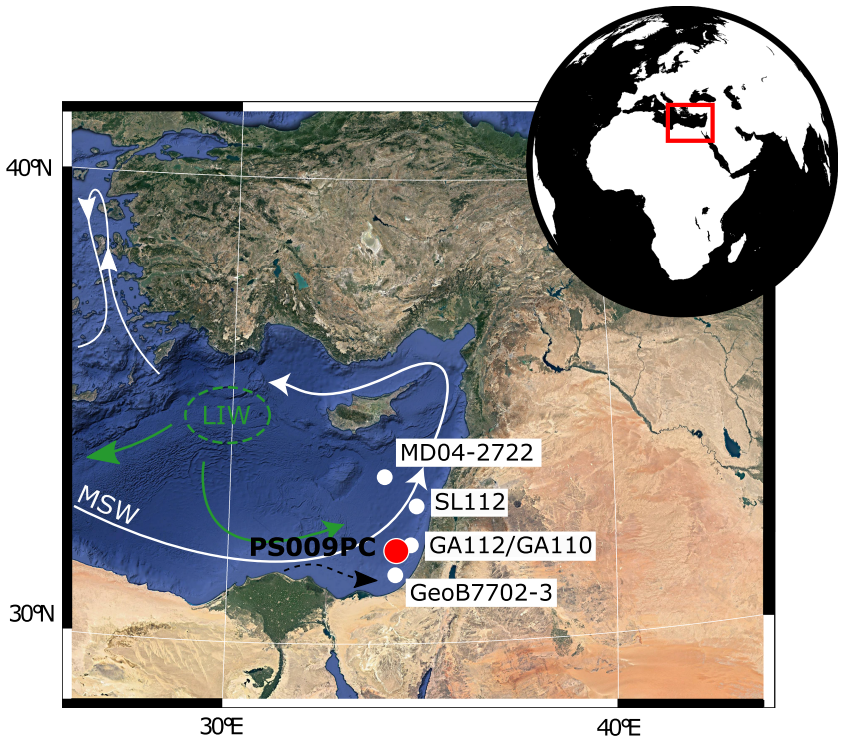

Figure 1. Geographical location of core PS009PC. Locations of the cores used in the text for discussion are indicated on the map: core PS009PC (32°07.7′N, 34°24.4′E; 552-m water depth), MD04-2722 (33°06′N, 33°30′E; 1,780-m water depth; Cornuault et al., 2016, 2018), SL112 (32°44.5′N, 34°39′E; 892-m water depth; Kuhnt et al., 2008), GA-110 (31°56.61′N, 34° 19.79′E, 670-m water depth; Schilman, Bar-Matthews, et al., 2001), GA-112 (31°56.41′N, 34°22.13′E, 470-m water depth; Schilman et al., 2001), and GeoB 7702-3 (31°39.1′N, 34°04.4′E, 592-m water depth; Castañeda et al., 2010). White arrows indicate the surface water current (MSW) and green arrows the intermediate water mass (LIW). Dashed arrow symbolizes the fresh water flux from the Nile River. The maps were made using the free software "NatGeo MapMaker."

2.2. Oceanographic Setting

The surface water (0- to 200-m water depth) of the Levantine Basin consists of eastward Mediterranean surface water (MSW), also called Modified Atlantic Water, which is diverted to the north along the EM coastline (Pinardi & Masetti, 2000). This anticlockwise flow is the major vector of sediment transport from the Nile River to the studied site. From 200- to 600-m depth, the Levantine Intermediate Water (LIW) mass is present. LIW is occasionally formed during cool winters that induce convection of MSW to intermediate depths in the Rhodes gyre (Ovchinnikov, 1984; Lascaratos, 1993; Lascaratos et al., 1993; Menna & Poulain, 2010; Nittis & Lascaratos, 1998). The LIW plays an important role in the Mediterranean Sea circulation as the warmest and saltiest Mediterranean water mass and because it is involved in the subsequent formation of deep water in the eastern and western Mediterranean basins (Millot & Taupier-Letage, 2005).

At a water depth of 552 m, our studied core is, today, mainly located at the transition between LIW and the Eastern Mediterranean Deep Water (Mojtahid et al., 2019). However, it may have been bathed by different water masses during the LGM that is characterized by a lower sea level or during the S1 period characterized by a reduced LIW formation (Cornuault et al., 2018; Freydier et al., 2001; Scrivner et al., 2004; Tachikawa et al., 2015; Wu et al., 2019).

2.3. Climatology

The climate of the Levantine Basin is highly variable as a result of the influence of both low and high latitudinal atmospheric systems interacting with the local and complex surrounding topography such as the Taurus, Zagros, and Amanos mountains (Evans et al., 2004; Lelieveld et al., 2012). The northern part of the EM is mostly temperate with warm to hot, dry summers and mild, relatively wet winters (Bolle, 2003; Lionello et al., 2006). In contrast, the southern part is characterized by an arid and hot desert climate with

low precipitation (Issar & Zohar, 2004). Therefore, the temperature, precipitation, and wind regimes present remarkable North-South geographical and seasonal gradients across the region. For instance, the wind-curl pattern responsible for the LIW formation responds to (i) the Atlantic westerlies during winter that gain moisture while moving eastward over the warm Mediterranean waters and (ii) the northwesterlies strengthened by the Aegean Etesian regime during summer (e.g., Bolle, 2003; Lionello et al., 2006). It is the outbreaks of cold and dry air into the Levantine Basin from the northern continental regions that lead to significant buoyancy losses initiating the formation of the LIW in winter (Lascaratos et al., 1993; Wüst, 1961). During summer, the northern position of the Azores subtropical high-pressure cell reinforces the dryness of the southern Levantine. This southern climatic system is modulated by the northeast African monsoon system, which controls the northward limit of the Intertropical Convergence Zone.

This northward penetration of the monsoonal rain belt, which in turn is affected by precession-forced insolation changes (Rohling, 1994; Rossignol-Strick, 1985), mainly controls the discharge of the Nile River into the Levantine Basin (Nicholson, 2009). Therefore, the Levantine area, being influenced by high Nile River sedimentation (Krom et al., 1999), is the ideal location to investigate the present and past dry/wet oscillations in the Mediterranean climate (e.g., De Lange et al., 2008; Peyron et al., 2017; Schilman, Almogi-Labin, et al., 2001).

3. Material and Methods

For consistency with the other proxy studies performed on core PS009PC (Hennekam et al., 2014; Mojtahid et al., 2015, 2019), we use the same age model. However, as that age model contained only the interval from 0 to 16.5 kyr (0–322.6 cm), we added one radiocarbon date (uncorrected ^{14}C age is 16,190 $\pm$ 80 years) at 382.6 cm. Using the same calibration strategy as described in Hennekam et al. (2014), we obtain a calibrated ^{14}C date of 19.0 ka for this depth, and we used a linear age-depth transition between 322.6 and 382.6 cm (supporting information, Figure S1).

The benthic foraminiferal fauna was analyzed in 178 subsamples with a 2-cm resolution corresponding to ~20 years (in the Late Holocene) to 160 years (during the Late Pleistocene). All subsamples were first wet weighed, and the dry weight was estimated using the sediment-water content, which was derived by wet and dry weighing of parallel samples (Hennekam & de Lange, 2012). Subsamples were washed through a 150-μm sieve. Although we are aware that small-sized adult species may compose a large part of the foraminiferal assemblage, the <150-μm fraction was not considered in this study. According to our experience in the Mediterranean Sea and the inspection of some of the studied samples from the <150-μm fraction, this latter contains mainly juveniles of the species found in the larger fraction, in line with findings of a study from a nearby location (Schmiedl et al., 2010). Because of the high foraminiferal abundances in some levels, samples were split into subsamples (aliquots) using an Otto Microsplitter. More than 200 specimens were picked out from a single aliquot using a binocular microscope, stored in separate Chapman slides, and identified at a species level. The absolute abundances were standardized per gram of dry sediment (ind/g), and species relative abundances (%) were calculated with a statistical minimal threshold of 10 individuals per sample. Here, we present only the species that are present with a relative abundance $\geq$5% in at least one sample. The complete raw data set is available in Table S1. The benthic foraminiferal accumulation rate (BFAR, ind/cm^2/ka) was calculated as the product of absolute abundance (ind/g), sedimentation rate (cm/ka), and dry bulk density (g/cm^3; Herguera & Berger, 1991). Principal component analysis (PCA) on covariance was performed using PAST software package (PAleontological STatistics, Version 3.25; Hammer et al., 2001) on (i) the relative abundances of the 33 major benthic species ($\geq$5%) and (ii) on the stable isotopic records of *Uvigerina mediterranea*, *Uvigerina peregrina*, and *G. ruber*. Diversity (Shannon *H*) index was calculated using the same software.

Stable oxygen ($\delta^{18}O$) and carbon ($\delta^{13}C$) isotopes were measured on the tests of three benthic species *Cibicidoides pachyderma*, *U. mediterranea*, and *U. peregrina*. Depending on their respective presence, one, two, or the three species were handpicked every 4 cm, except for the first part of the sapropel period where these were rare. Approximately ~5–10 tests of the benthic species were handpicked from the 250- to 300-μm fraction. For planktic foraminiferal oxygen and carbon stable isotopes, most of the data (13–0 ka) are published in Hennekam et al. (2014) and Mojtahid et al. (2015). Here, we performed 107 additional carbon and oxygen isotope measurements on the same planktic species *G. ruber* (white, sensu stricto) to extent

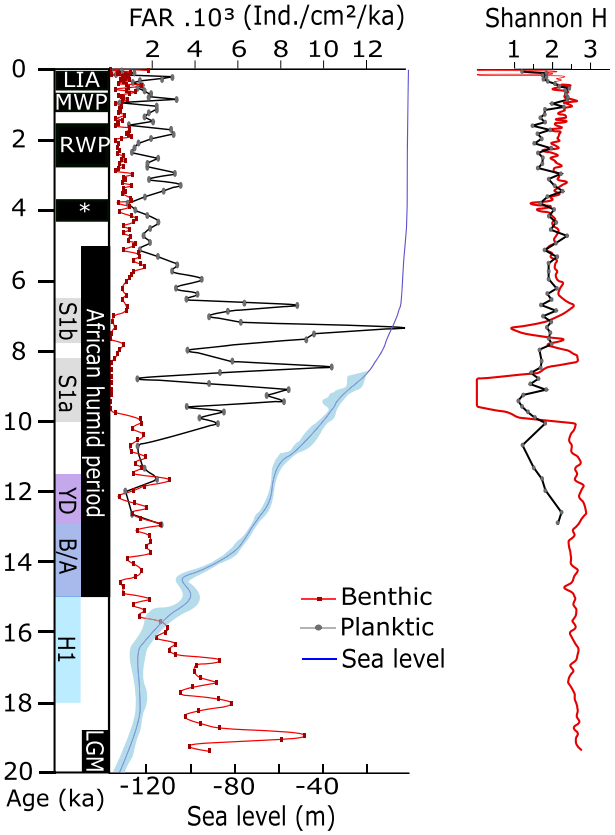

Figure 2. Foraminiferal accumulation rate and diversity of core PS009PC. Foraminiferal accumulation rate (FAR, ind/cm^2/ka) and Shannon (*H*) diversity index for both planktic (Mojtahid et al., 2015) and benthic foraminifera (this study). The reconstructed relative sea-level curve (Fleming et al., 1998; Lambeck et al., 2014) is represented. B/A: Bølling-Allerod; H1: Heinrich 1; LGM: Last Glacial Maximum; LIA: Little Ice Age; MWP: Medieval Warm Period; RWP: Roman Warm Period; S1a & S1b: the two phases of sapropel 1 event; YD: Younger Dryas. "*" marks the "4.2 ka cal BP" event (Bar-Matthews et al., 1997, 1999; Bartov et al., 2003; deMenocal, Ortiz, Guilderson, Adkins, et al., 2000; Essallami et al., 2007; Ehrmann et al., 2007; Kotthoff et al., 2008; Dormoy et al., 2009; Almogi-Labin et al., 2009; Castañeda et al., 2010; Gasse et al., 2011; Revel et al., 2014; Hennekam et al., 2014).

the previous record to 19 ka (i.e., from 279 to 392 cm with a ~1-cm resolution (Table S2). The methodology used for planktic and benthic species is detailed in Hennekam et al. (2014). The δ^{13}C and δ^{18}O were measured with a Finnigan MAT-253 mass spectrometer coupled to a Kiel-III carbonate preparation device at the University of Utrecht for *U. mediterranea*, *U. peregrina*, and *G. ruber* and at the Pôle spectrometrie Océan (Brest, France) for *C. pachyderma*. The standard deviation is ±0.04‰ for δ^{13}C and ±0.06‰ for δ^{18}O obtained from 196 measurements of the NBS-19 standard. The δ^{18}O and δ^{13}C isotope measurements are reported in per mille relative to the Vienna Pee Dee Belemnite.

To infer productivity changes, we use the difference between the δ^{13}C of planktic (*G. ruber*) and benthic foraminifera (*U. mediterranea*; $\Delta\delta^{13}$Cp-b) and the difference between the δ^{13}C of the epifaunal to very shallow benthic infaunal species *C. pachyderma* and the shallow to intermediate infaunal species *U. mediterranea* ($\Delta\delta^{13}C_{pachy\text{-}med}$) as suggested in previous studies (McCorkle et al., 1990, 1997; Schilman, Almogi-Labin, et al., 2001, 2003). High values of $\Delta\delta^{13}$Cp-b indicate high sea surface productivity because high photosynthetic activity leads to a depletion of ^{12}C in surface water and subsequently to higher δ^{13}C of planktic foraminifera. Meanwhile, the remineralization of ^{12}C-enriched phytodetritus in the deep-sea water column and sediment induces a decrease in the benthic δ^{13}C values. Within the sediment, the pore water δ^{13}C gradient depends on the quantity of organic matter arriving to the seafloor and reflects its degradation in the top sediment layers (McCorkle et al., 1990, 1997). As such, high values of $\Delta\delta^{13}C_{pachy\text{-}med}$ indirectly indicate high sea-surface productivity, although the application of this proxy can be complicated by lateral advection of terrestrial organic matter in marginal settings (Theodor, Schmiedl, Jorissen, et al., 2016). Because oxygen consumption and the degradation of organic matter are two interlinked parameters that are difficult to decipher, the $\Delta\delta^{13}$Cp-b can also be used as a proxy for oceanic ventilation (Loubere, 2001; Spero & Lea, 2002). As such, an active bottom water ventilation with relatively high δ^{13}C-DIC signature (compared to aged waters with low δ^{13}C-DIC) will reduce the $\Delta\delta^{13}$Cp-b values. In addition, the $\Delta\delta^{13}$Cp-b values can also be reduced in near-river locations, such as our study site, by the introduction of isotopically light DIC to surface waters, originating from riverine influx of remineralized terrestrial material decreasing the planktic δ^{13}C signature (e.g., Casford et al., 2002; Mojtahid et al., 2015).

The REDFIT and continuous wavelet transform (Morlet wavelet) analyses were processed using PAST software to shed light on the frequency embedded in the relative abundance spectrum. The spectral analyses were done using pretreated data as follows: (i) at first, a 3-point average was applied to smooth the noise that is inherent to the method and to intraspecies and interspecies differences; (ii) then, the records were linearly interpolated at even spaced time resolution (100 years); and (iii) to finish, the data were band-pass filtered to stop low-frequency variability (wavelengths >3 ka) in order to focus on multicentennial timescale variability.

4. Results

4.1. Benthic Foraminiferal Fauna

The BFAR ranges from 0 to 9,141 ind/cm^2/ka, showing an overall decreasing trend since ~19 ka. The highest values are recorded in the interval before 15 ka, and the lowest values are found during sapropel S1 (Figure 2). Shannon index values range between 0.5 and 3. The lowest diversities are found during S1

with an interruption at ~8.2 ka (Figure 2). These two phases are synchronous to S1a and S1b events, determined from geochemical properties, with the lowest Shannon index recorded during S1a and a rebound of the diversity index during the S1 interruption at around 8.2 ka.

For the whole record, 33 species dominate the assemblages (>5%). These were separated into three statistical groups based on the PCA analysis (see Figure S2): (i) the post-sapropel group, (ii) the glacial-deglaciation group, and (iii) the Holocene-sapropel group. Figure 3 shows the relative and absolute abundances of the main species in each of these groups. This clearly highlights that (i) the species of the post-sapropel group are present all along the record but reach their maximum after S1, (ii) the species from the glacial-deglaciation group are largely dominant before S1, and (iii) the species from the Holocene-sapropel group are nearly exclusively found during S1. Based on the faunal assemblage, the oxygen-deficient interval associated to sapropel S1 is defined between 10.1 and 6.5 ka with a reoxygenation event occurring between ~8.6 and 7.8 ka.

In order to better highlight the trends of individual taxa, we identified key time periods in which some of the main benthic species present the most noticeable changes (Figure 4). The time period before sapropel S1 records three main changes: (i) from ~19 to 15.5 ka, the community was mainly represented by *U. peregrina*, *Bulimina marginata*, and *Hyalinea balthica*; (ii) from ~15.5 to 13 ka, the population was dominated by *U. mediterranea* and *Gyroidina altiformis*; and (iii) from ~13 to 10 ka, *U. mediterranea* was still the dominant species but seconded this time by *Bulimina inflata/striata* and *B. marginata*.

Through sapropel S1 (from ~10.1 to 6.5 ka), *Chilostomella oolina* was the most abundant species. However, benthic assemblage changed through this event with the dominance of *Globobulimina affinis* during S1a (from ~10.1 to 8.8 ka), the strong presence of *G. altiformis/orbicularis*, *B. inflata/striata*, and *U. mediterranea* between 8.8 and 7.7 ka, and the strong presence of *U. peregrina* and *G. orbicularis* during S1b (from ~7.7 to 6.5 ka).

After S1, the benthic foraminiferal community largely evolved: (i) from ~6.5 to 5 ka, the assemblage was dominated, in order of importance, by *U. peregrina, B. marginata*, and *G. orbicularis*; (ii) from ~5 to 3.5 ka, *B. marginata* was the most dominant species together with *U. peregrina* and *C. pachyderma*; (iii) from ~3.5 to 1.9 ka, *U. peregrina* became again the most abundant species with *B. marginata* and *B. inflata/striata*; (iv) from ~1.9 to 0.7 ka, *U. mediterranea* and *C. pachyderma* seconded *U. peregrina*; and (v) from ~0.7 ka to modern time, the assemblage was mainly represented by *U. peregrina* and *B. inflata/striata* with a relative high presence of *U. mediterranea*, *B. marginata*, and *C. pachyderma*.

4.2. Stable Isotope Records

Benthic foraminiferal $\delta^{18}O$ records of *U. mediterranea* and *U. peregrina* present an overall decreasing trend from ~4.5‰ to 2‰ between ~19 and ~8 ka followed by stable values at around 2‰ until modern time. Measurements obtained from *C. pachyderma*, between ~15 and 13 ka and over the last 5 kyr, do not show a specific trend (Figure 5a). More specifically, the continuous $\delta^{18}O$ record obtained from *U. mediterranea* shows variability throughout the glacial termination (while *U. peregrina* was not present from ~17 to 8 ka). The $\delta^{18}O$ of *U. mediterranea* is around 4.5‰ during the LGM, and then it decreases by 1‰ over the H1 event and rises back through the B/A event to reach the value of 4‰ at around 12 ka, corresponding to the middle of the Younger Dryas time period.

In terms of absolute values, the $\delta^{13}C$ values of *U. peregrina* are systematically lower by ~1.5‰ than *U. mediterranea*, which in turn shows lower $\delta^{13}C$ values by ~0.6‰ than *C. pachyderma* (Figure 5b). The $\delta^{13}C$ record of *U. mediterranea*, which is the more continuous record over the last 19 ka, shows six distinctive time periods: (i) from 20 to 17 ka, the $\delta^{13}C$ values are relatively constant at around 0.75‰ (0.25‰ for *U. peregrina*); (ii) from 17 to 15 ka, during the H1 event, the $\delta^{13}C$ is relatively stable until 17 ka and then shows a positive excursion (~0.5‰) centered at around 16 ka; (iii) from 15 to 13 ka, encompassing the B/A period, the $\delta^{13}C$ decreases to reach 0.2‰; (iv) from 13 to 11.5 ka, corresponding to the YD event, the $\delta^{13}C$ shows a positive excursion, up to +0.5‰; (v) from 10 to 6 ka, during S1, the $\delta^{13}C$ is at its minimum value of −0.3‰ (also for the *U. peregrina*'s $\delta^{13}C$, at −1.7‰). Both *U. peregrina* and *U. mediterranea* records reach their minimum value at around 7 ka, during the S1b. (vi) After 6.5 ka, the $\delta^{13}C$ strongly oscillates between ~0‰ and 1‰ for *U. mediterranea* and between approximately −1.5‰ and −0.5‰ for *U. peregrina*, while for the *C. pachyderma*, the variability is low (i.e., less than 0.3‰).

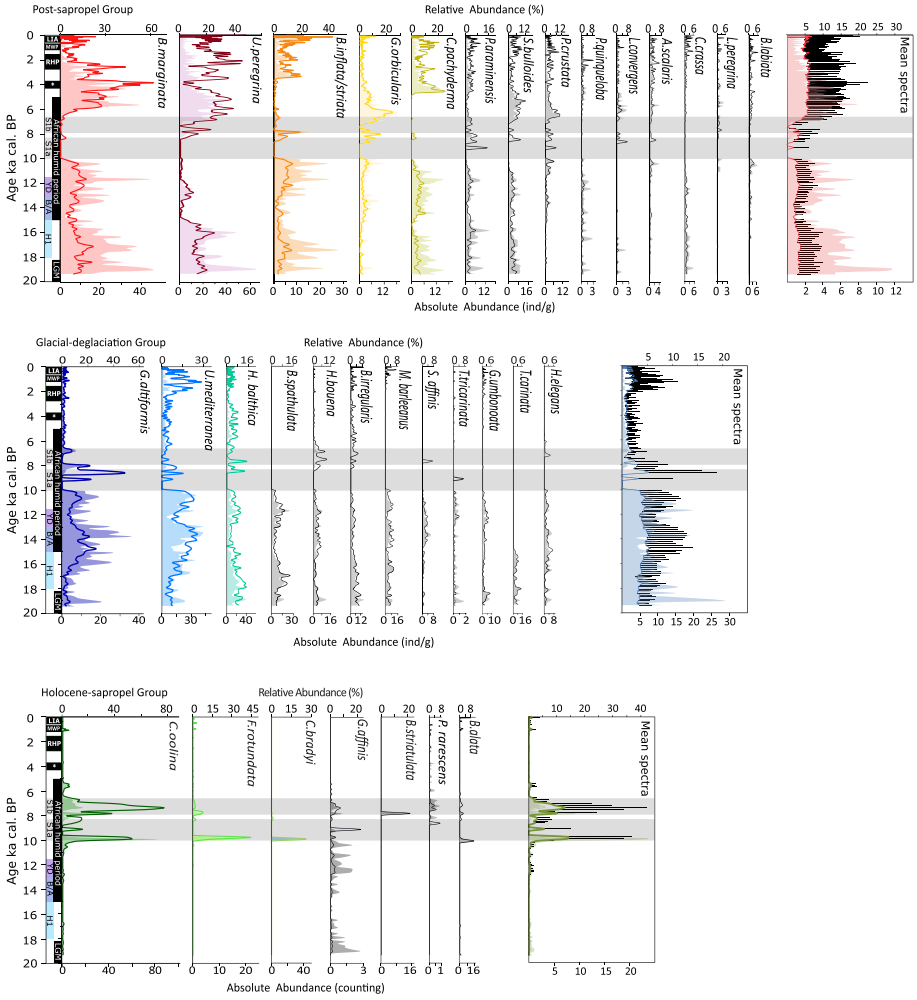

Figure 3. Absolute and relative abundances of the main (≥5% of total abundance) benthic foraminiferal species. These are organized following the three PCA groups (see Figure S2). The full lines represent the relative abundances (%), while the color-shaded surfaces represent the absolute abundances (ind/g). For each PCA group, species were ordered according to their mean percentages in the entire record, from the highest to the lowest (only the spectrum of the discussed species was colored). The mean spectra are shown on the right for each of the three PCA groups, and the error bars represent the associated standard deviation. The main events and climate phases are reported similarly to Figure 2.

5. Discussion

5.1. Ecology of the Main Benthic Foraminiferal Species

The PS009PC benthic species composition is characterized by the dominance of *B. marginata/inflata/striata*, *U. peregrina/mediterranea*, *H. balthica*, *C. pachyderma*, *G. altiformis*, and *C. oolina* (Figure 3). Because these species are known to have different ecological requirements in the EM (e.g., De Rijk et al., 2000; Schmiedl et al., 2010), we interpret their changes in relative abundances, mainly in terms of changes in carbon export and productivity and, in some cases, in terms of oxygenation.

B. marginata, *H. balthica*, and *U. peregrina* are generally considered as meso-eutrophic species (e.g., Fontanier et al., 2003; Koho et al., 2008; Murray, 2006), and in the Atlantic and Mediterranean, *U. peregrina* and *U. mediterranea* respond to high organic matter flux (Fontanier et al., 2008) >10 g/cm^2/year (Altenbach et al., 1999; De Rijk et al., 2000). Although they are both linked to high food quality, *B. marginata* is considered to be less opportunistic than *U. peregrina* (De Rijk et al., 2000; Murray, 2006). In the nearby core SL112, albeit not based on experimental nor in situ evidence, Schmiedl et al. (2010) hypothesized that *U. peregrina* responds to seasonal phytodetritus pulses triggered either by summer Nile flood peaks or by enhanced

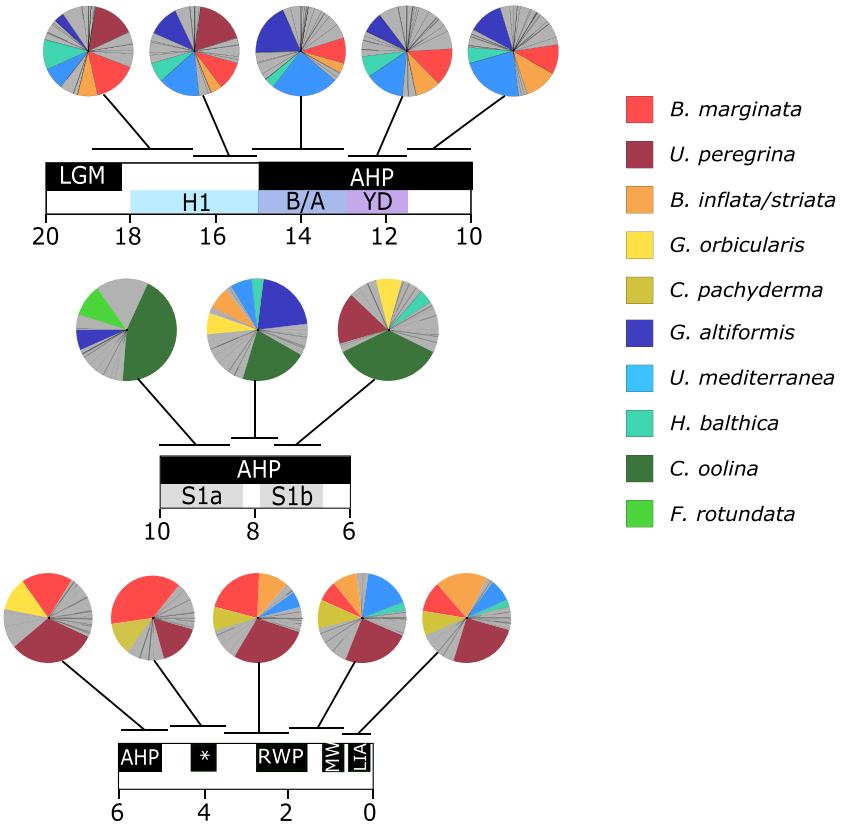

Figure 4. Pie chart analyses of benthic foraminiferal community. The pie charts present the relative abundances of the dominant species (≥5%) averaged for the selected time periods. Only the dominant species showing the most noticeable changes are represented in colors (see also Figure 3), and the other species are undifferentiated and represented in grey. The main events and climate phases are reported similarly to Figure 2.

winter-spring wind-induced mixing, while *U. mediterranea* might be able to feed on more degraded food sources. In our record, as in the nearby cores GA-112 and GA-110 (Schilman et al., 2003), *U. mediterranea* is also shown to be highly sensitive to changes in the degree of organic matter degradation, and therefore, its high abundance will be used as reflecting periods of enhancement of refractory organic matter input, while *U. peregrina* will be used to infer periods of high primary productivity.

The $\delta^{13}C$ signal of *U. peregrina* is systematically lower than the $\delta^{13}C$ *U. mediterranea* by around 1‰. Such difference between species is often interpreted as reflecting the species vertical distribution in the sediment such as the deepest microhabitats being characterized by the lowest $\delta^{13}C$-DIC signature of pore waters as a result of organic matter mineralization (e.g., Fontanier et al., 2006; Schilman et al., 2003). However, in the Mediterranean Sea, *U. peregrina* and *U. mediterranea* can be found in similar microhabitats (Fontanier et al., 2008; Schmiedl et al., 2000), but the $\delta^{13}C$ signature of *U. peregrina* was shown to contain a stronger vital effect as it is close to that of the $\delta^{13}C$ of the deep infauna (Schmiedl et al., 2004, Theodor, Schmiedl, & Mackensen, 2016). Consequently, and as also suggested by Fontanier et al. (2002), we are not using the $\delta^{13}C$ of *U. peregrina* for our $\delta^{13}C$-DIC interpretations. The epibenthic to very shallow infaunal *C. pachyderma* would be a more appropriate recorder, although in our case, a continuous record is only available for the Late Holocene (Figure 5). Furthermore, the $\delta^{13}C$ range of variability of *C. pachyderma* is very low (0.3‰) compared to the other species (~0.8‰) confirming a lesser reactivity to organic matter input. For these reasons, we are using the $\delta^{13}C$ of *U. mediterranea* as representing the $\delta^{13}C$-DIC of pore waters. This gives us a first approximation of bottom water $\delta^{13}C$-DIC as the latter also depends on the organic matter flux rate (Theodor, Schmiedl, & Mackensen, 2016).

The sapropel event is marked by the occurrence of species known to be tolerant to low-oxygen conditions (Jorissen, 1999; Schmiedl et al., 2010) such as *C. oolina*, *G. affinis*, *C. bradyi*, and *F. rotundata* (Figure 3). However, this episode is also punctuated by the presence of species such as *G. altiformis/G. orbicularis*,

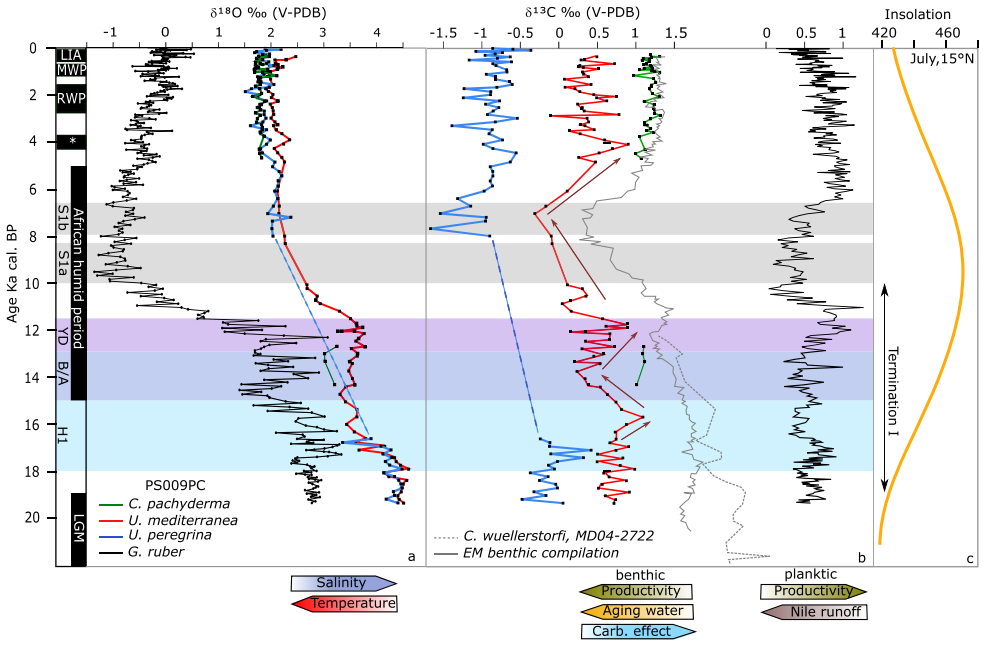

Figure 5. Stable isotopes foraminiferal records in core PS009PC. (a) Oxygen stable isotopic records obtained from *C. pachyderma*, *U. peregrina*, *U. mediterranea* (this study), and *G. ruber* (Hennekam et al., 2014; Mojtahid et al., 2015; and this study from 13 to 19 ka). (b) Carbon stable isotopic record obtained from the same species. The red arrows underline the main feature of the benthic $\delta^{13}C$ record discussed in the text. The MD04-2722 $\delta^{13}C$ record is from Cornuault et al. (2016), and the EM benthic compilation is extracted from Grimm et al. (2015). (c) June insolation at 15°N is reported along the studied time period (Berger & Loutre, 1991). The Termination I is defined between ~19 and 10–11 ka (e.g., Denton et al., 2010; Raymo, 1997). The main events and climate phases are reported similarly to Figure 2. The arrows at bottom of figures indicate potential processes associated with changes in isotopic composition: productivity in surface water, Nile River activity, carbonate ion effect and ventilation (more or less aging waters) for the $\delta^{13}C$, and salinity and temperature for the $\delta^{18}O$.

which are typical oligotrophic species (De Rijk et al., 2000, Hyams-Kaphzan et al., 2018) and classified as oxyphilic species in the study of Schmiedl et al. (2010) from the EM. Similar to Schmiedl et al. (2010), we use the presence of *Gyroidina* spp. through S1 event as an indicator of reoxygenation episodes.

5.2. Changes in Surface Productivity and Organic Matter Flux

The major changes in the benthic foraminiferal community mainly occur during three contrasting time periods: the glacial-deglaciation, Holocene-sapropel, and post-sapropel/Holocene intervals. This is in line with earlier studies from the EM for this time period (Abu-Zied et al., 2008; Drinia et al., 2016; Kuhnt et al., 2007; Louvari et al., 2019; Schmiedl et al., 2010). In our study, this subdivision is clearly expressed in the community changes (Figure 3), in the BFAR and diversity index (Figure 2), and in the stable carbon and oxygen isotopes (Figure 5). Hereafter, we discuss in detail the three major changes in benthic faunal groups (glacial-deglaciation, Holocene-sapropel, and post-sapropel, see Figure 3) along with the planktic-based proxies obtained from the same studied core (Hennekam et al., 2014; Mojtahid et al., 2015).

5.2.1. The Glacial and Deglaciation Conditions

In our record, the BFAR shows its maximum values during a period of a relatively low sea-level stand (until 16.5 ka), encompassing the LGM and the beginning of H1 (Figure 2). During these two time intervals, the benthic community remained generally unchanged and is dominated by the meso-eutrophic and opportunistic *B. marginata*, *H. balthica*, and *U. peregrina* (Figures 3 and 4). Therefore, we hypothesize that this benthic community indicates a maintained high trophic level over the LGM and the beginning of H1. A high trophic level is coherent with the low sea-level stand at the time, resulting in shallower benthic habitats and a narrower continental shelf. This latter resulted potentially in larger inputs of continental organic matter and nutrients. In this case, the introduction in surface waters of isotopically light $\delta^{13}C$ terrestrial material might explain the low $\Delta^{13}Cp\text{-}b$ recorded during this period (Figure 6).

The BFAR decreased significantly at the onset of the sea-level rise that occurred from the mid-H1 event, at ~16.5 ka, to its end, at ~15 ka (Figure 2). At that time, a significant change in the benthic faunal community

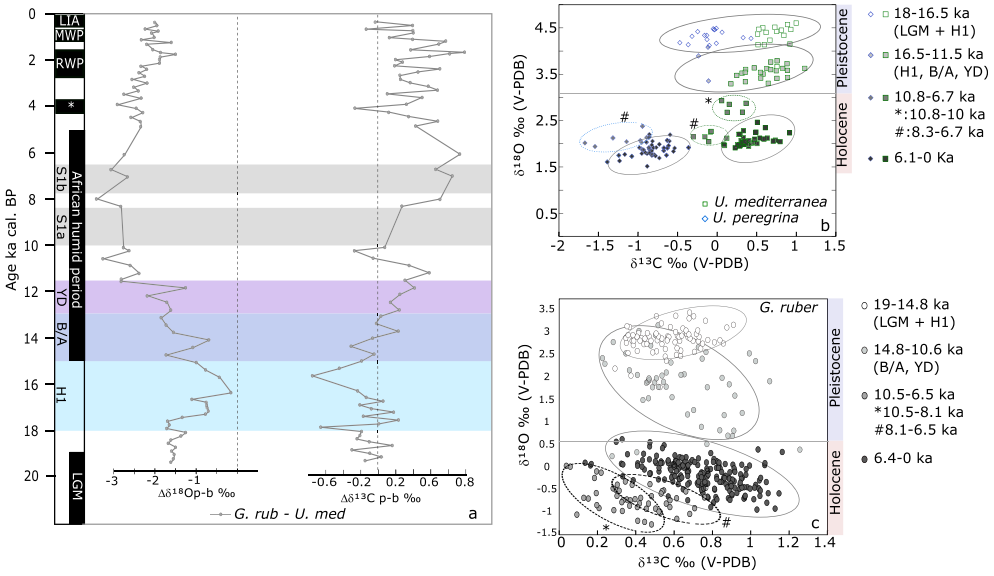

Figure 6. δ^{18}O-δ^{13}C benthic-planktic coupling in core PS009PC. (a) $\Delta\delta^{18}$O and $\Delta\delta^{13}$C records. $\Delta\delta^{18}$Op-b and $\Delta\delta^{13}$Cp-b represent respectively the difference between the oxygen and the carbon isotopic records of *U. mediterranea* and *G. ruber* for the same lithological level. (b) δ^{18}O-δ^{13}C crossplot from the benthic *U. peregrina* and *U. mediterranea* foraminiferal records (this study) and from the *G. ruber* planktic foraminiferal records (data from Hennekam et al., 2014 and this study for the 13- to 19-ka interval). Clusters were based on PCA analyses (Figure S3).

occurred, with *U. mediterranea* becoming the dominant species while *U. peregrina* almost vanished from the assemblage (Figure 7a). This community transition is also found in the nearby core SL112 (Figure 7a), albeit it was not discussed in detail in Schmiedl et al. (2010). On the Eastern region of the North Africa, H1 is expressed as a dry interval resulting from a southward shift in the monsoon rain belt and consequently a reduction in summer rainfall intensity (Revel et al., 2015; Shanahan et al., 2015). This would be consistent with a relative decrease in Nile River runoff and nutrient input (Bout-Roumazeilles et al., 2007; Dormoy et al., 2009; Nebout et al., 2009). An environment with low nutrient inputs results in low primary production at the surface and consequently low export of phytodetritus to the bottom. This might explain both the planktic δ^{13}C decrease and the benthic δ^{13}C increase recorded from ~16.5 to 15.7 (Figure 5), together with the decrease of the abundance of the eutrophic *U. peregrina* species (Figure 7a).

Remarkably, between ~13 and 11 ka, the low presence of *U. mediterranea* is synchronous with a slight rebound in the occurrence of *U. peregrina* as well as with an increase in the benthic δ^{13}C record (Figure 7a). Simultaneously, we record a relatively high presence of the other eutrophic species, that is, *B. marginata/inflata/striata* (Figures 3 and 4), along with a highly diverse planktic foraminiferal fauna characterized by the presence of the opportunistic *Globigerina bulloides* (Mojtahid et al., 2015). For this time interval, which coincides with the arid and cold YD (deMenocal, Ortiz, Guilderson, Adkins, et al., 2000), both surface and bottom water ecological indicators point to an enhancement of the surface productivity in our study area, similarly to what have been observed in other sub-basins of the EM (e.g., Geraga et al., 2008; Triantaphyllou et al., 2009). However, because the Nile River runoff is known to be low during the YD in the area (deMenocal, Ortiz, Guilderson, Adkins, et al., 2000), this high surface productivity might be the result of intensified wind activity (Box et al., 2008; Robinson et al., 2006), which might have fertilized surface waters by either dust input or enhanced surface water mixing. Isotopically, both planktic and benthic δ^{13}C records increase progressively (~+0.7‰) through the YD (Figure 5a). While the planktic signal corroborates an increase in surface productivity, the increasing benthic δ^{13}C values (Δ^{13}Cp-b ~ 0) suggest that bottom water processes act independent from surface productivity (discussed further in section 5.3).

5.2.2. Sapropel Conditions

During S1, the BFAR and the Shannon diversity index (*H*) drop drastically (Figure 2). This is likely due to the low bottom water oxygen conditions that characterized the deep basins of the eastern Mediterranean Sea during this episode, resulting from a highly stratified water column (e.g., Grimm et al., 2015) and/or high organic

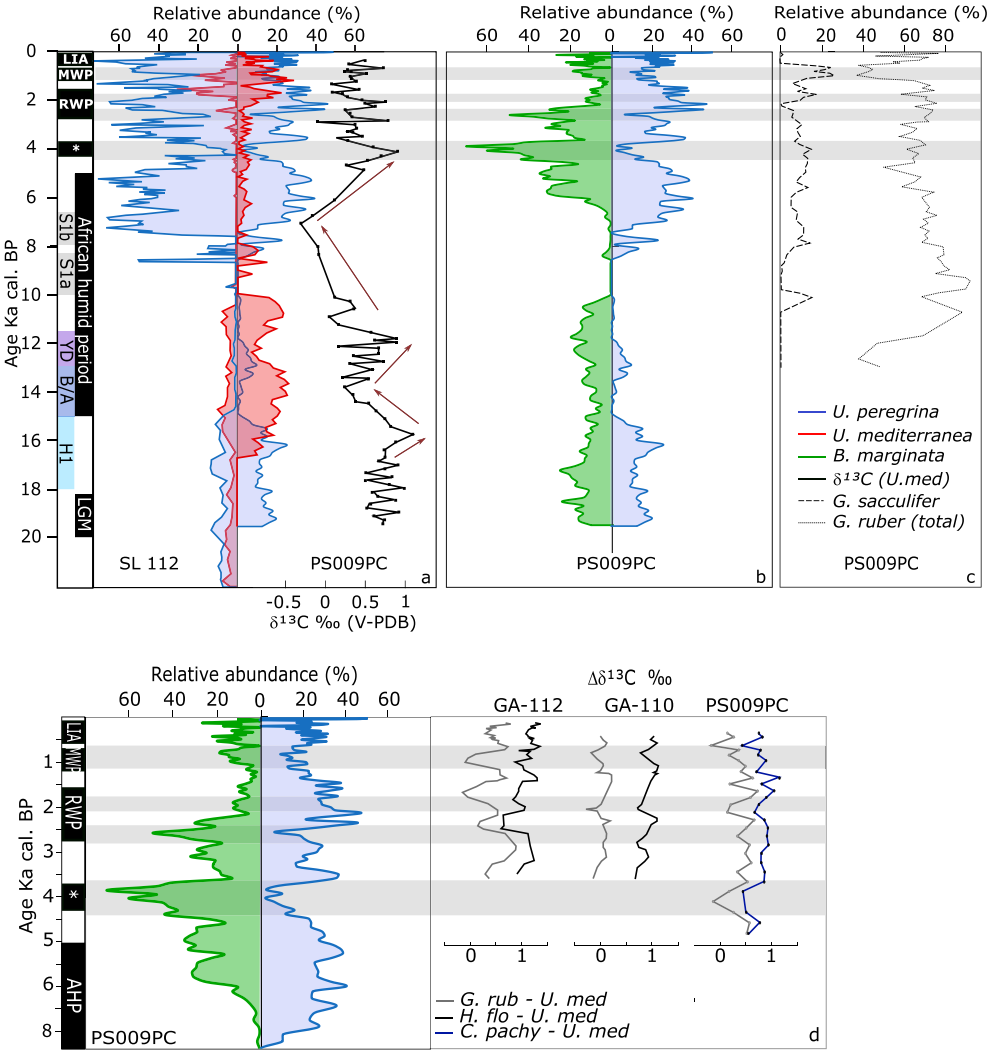

Figure 7. Relative abundance of key species in the Levantine Basin. (a) Relative abundances of *U. peregrina* and *U. mediterranea* in core SL112 (Schmiedl et al., 2010) and core PS009PC (this study) and $\delta^{13}C$ measured on *U. mediterranea* from core PS009PC (this study). The red arrows mark the main features of the $\delta^{13}C$. (b) Relative abundances of *U. peregrina* and *B. marginata* from core PS009PC (this study). (c) Relative abundance of *G. ruber* and *G. sacculifer* from core PS009PC (Mojtahid et al., 2015). The main events and climate phases are reported similarly to Figure 2, and the three shaded time periods underline the Holocene dry episodes as discussed in the text. (d) $\Delta\delta^{13}C$ comparison between PS009PC core and the nearby GA-112 and GA-110 cores (Schilman, Almogi-Labin, et al., 2001, 2003) along the benthic faunal assemblages. *C. pachy: C. pachyderma*; *G. rub*: *G. ruber*; *H. flo: Heterolepa floridana*; *U. med: U. mediterranea*. To overcome the difference in resolution between the compared benthic and planktic species in PS009PC, the $\Delta\delta^{13}C$ was calculated from $\delta^{13}C$ values averaged from five successive lithological levels for the three considered species.

matter input (De Lange et al., 2008). These processes are corroborated by the planktic data from the same core showing that the S1 interval is characterized by a maximal value of the PFAR (Figure 2), which was interpreted as indicating high primary production, and low values of $\delta^{13}C$ were interpreted as increased input of isotopically light terrestrial material (Mojtahid et al., 2019). Despite these low-oxygen conditions, benthic foraminifera do not completely vanish, highlighting a variability in bottom oxygen content (Figure 3). The intermittent presence of *C. oolina*, *G. affinis*, *C. bradyi*, and *F. rotundata* indicate intervals of low-oxygen conditions, while the occurrence of oxyphilic species such as *G. altiformis/orbicularis*, *B. inflata/striata*, and *U. peregrina/mediterranea* indicate episodes of reoxygenation (De Rijk et al., 2000; Schmiedl et al., 2000, 2010; Figures 3 and 4). These reoxygenation events are likely so well expressed at this site due to the shallow depth of 552 m (e.g., Mojtahid et al., 2019). The consistent occurrence of oxyphilic species from 8.6 to 7.8 ka indicates a major period of reoxygenation during sapropel S1 (Figure 4). This interruption, usually correlated to the Northern Hemisphere cold 8.2-ka event, is also

recorded in the Aegean and Adriatic Seas (e.g., Casford et al., 2003; De Rijk et al., 1999; Giamali et al., 2019; Incarbona et al., 2019; Kontakiotis et al., 2016; Marino et al., 2009; Rohling, Mayewski, et al., 2002; Siani et al., 2010, 2013; Triantaphyllou et al., 2009, 2016). Several studies proposed that the 8.2-ka interruption during S1 formation is due to a more pronounced Siberian high-pressure system (e.g., Pross et al., 2009; Rohling, Mayewski, et al., 2002; Schmiedl et al., 2010), combined with a southward migration of the Intertropical Convergence Zone weakening the monsoon systems (e.g., Fleitmann et al., 2007; Triantaphyllou et al., 2009). The time interval for the reoxygenation event based on benthic foraminiferal abundances is slightly longer than the S1a/S1b interruption (8.2 to 7.9 ka, Figure 3) defined by sedimentary Ba/Al (a geochemical proxy for export productivity) from the same core PS009PC (Hennekam et al., 2014). This may corroborate earlier findings showing the high importance of re-ventilation (vs. a decrease in productivity) for the cause of this event.

The reappearance of *U. peregrina* together with the freshwater-intolerant planktic taxon *G. sacculifer* during S1b indicates less severe environmental conditions compared to S1a as previously suggested by Hennekam et al. (2014) and Mojtahid et al. (2015). Both planktic and benthic data indicate high river runoff, enhanced input of terrestrial organic matter, and overall low bottom oxygen conditions with intermittent reoxygenation events (Figure 8).

5.2.3. Post-Sapropel Conditions

During the Holocene, after the end of the sapropel, largest variability in the benthic community mainly occurs in three species: *U. peregrina*, *U. mediterranea*, and *B. marginata* (Figures 3 and 4). In the nearby core SL112, *U. peregrina* showed an opposite pattern compared to *U. mediterranea* (Schmiedl et al., 2010). In our study core PS009PC, this opposite pattern in these two benthic foraminifers is less obvious (Figure 7a). Our data especially show that the opportunistic and eutrophic *U. peregrina* alternates asynchronously with the less opportunistic and eutrophic *B. marginata* (Figure 7b). Therefore, even if the bottom environment can be still considered as overall eutrophic over this time period, those oscillations might reflect the quality/nature of phytodetritus exported to the seafloor.

Interestingly, the periods of low-*U. peregrina*/high-*B. marginata* abundances are centered around 4.0, 2.5, 1.9, and 0.7 ka, which may correspond to specific climate events (Figure 7). The first episode coincides approximately with the so-called 4.2-ka BP event, a dry event in the Mediterranean region that may have played a large role in the collapse of the Old Kingdom of Egypt (Cullen et al., 2000) and is associated with a weakened Indian monsoon (Dixit et al., 2014) and low Nile discharges (Adamson et al., 1980; Hassan, 1997). The second and third periods coincide with the onset and the end of the RWP (Figure 7b). While this event is recorded in the North Atlantic and western Mediterranean as a more humid period (Cullen, 1981; Mojtahid et al., 2013), dry conditions seem to have prevailed in the eastern Mediterranean region (e.g., Avnaim-Katav et al., 2019; Giamali et al., 2019; Mojtahid et al., 2015; Schilman, Bar-Matthews, et al., 2001; Revel et al., 2014). In this area, this time period is also linked to a decrease in the Nile River flood discharges starting between 3.1 and 2.8 ka (Nicholson & Flohn, 1980; Woodward et al., 2008). Even though the time resolution is lower for planktic assemblages, the discussed arid 4.2-ka BP event and the RWP are also characterized by the relatively high occurrence of the oligotrophic planktic taxon *G. ruber* (Figure 7c) and a drop in diversity indicating low primary production (Mojtahid et al., 2015). The Medieval Warm Period (~1.1–0.54 ka) seems to match the last major drop at ~0.7 ka in *U. peregrina*'s abundance. This time period is known to have a strong regional hydrological variability. While arid conditions prevailed in the western Mediterranean (Martín-Puertas et al., 2010; Nieto-Moreno et al., 2011), several studies show that the climate is more humid towards the Levantine region (Frumkin et al., 1991; Schilman, Bar-Matthews, et al., 2001). Other studies show a more complex pattern within the Levantine area itself. In the East Levant (Syria, Israel), studies reported warm and humid conditions (Frumkin et al., 1991; Kaniewski et al., 2011; Schilman, Bar-Matthews, et al., 2001), while there are studies that point to dryer conditions at around 1 ka in the south Levant region and in the Nile catchment area (Flaux et al., 2012; Macklin et al., 2015; Revel et al., 2015). Additionally, the MWP episode is very different from the two previous "dry" events because while the benthic record indicates a less eutrophic environment (i.e., less *U. peregrina* and *B. marginata*), planktic foraminifera show an opposite signal. During the MWP, the abundance of oligotrophic *G. ruber* strongly decreases, and the high occurrence of *G. sacculifer* (Figure 7c) together with the eutrophic *G. bulloides* and the deep dwelling neogloboquadrinids mark a clear shift towards productive and well mixed surface waters (Mojtahid et al., 2015). When comparing our observations with the study of Schilman et al. (2003)

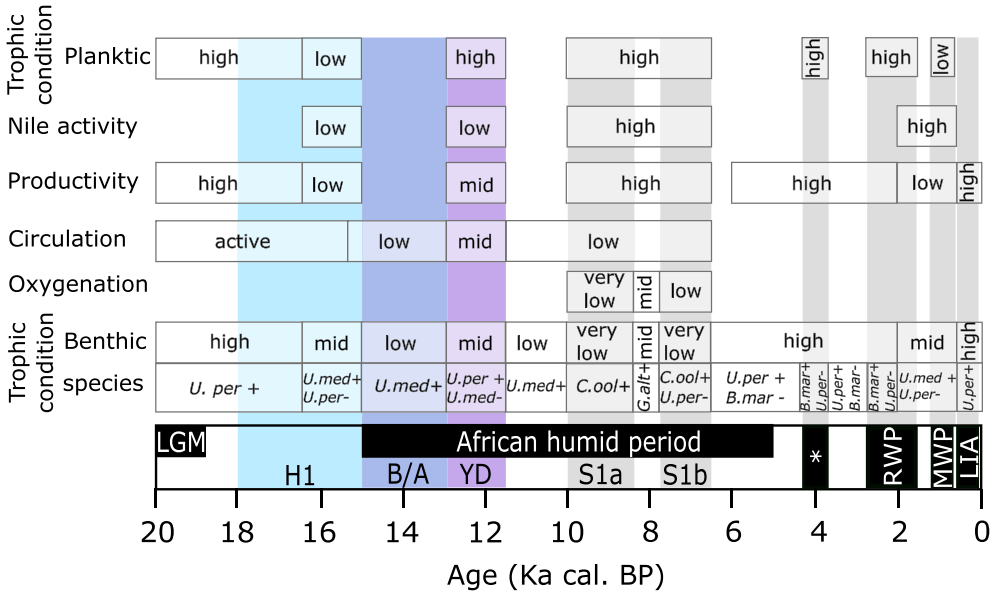

Figure 8. Summary scheme of the main environmental interpretations occurring in the EM since the last 19 ka. *B. mar: B. marginata*; *C. ool: C. oolina*; *U. med: U. mediterranea*; *U. per: U. peregrina*. The main events and climate phases are reported similarly to Figure 2.

that uses $\Delta\delta^{13}C$ in foraminifera from a nearby core (GA-112; Figure 7d), our low-*U. peregrina*/high-*B. marginata* intervals correspond with low $\Delta\delta^{13}C$ events in their core. They interpreted these intervals as periods of decreased productivity in the EM sea surface waters (Figure 7d). However, when applying the $\Delta\delta^{13}C$p-b and the $\Delta\delta^{13}C$*pachy-med* in our record, these oscillations are no longer present, and they are also very much attenuated (even absent) in the deeper nearby core GA-110 (670 m; Figure 1) according to the same study of Schilman et al. (2003; Figure 7d). This discrepancy might be explained in terms of a difference in water depths possibly affecting the path of the organic carbon to the seafloor as hypothesized by Schilman et al. (2003). The shallowest core (GA-112, 470 m) is potentially more influenced by the Nile river inputs than the two deeper cores (GA-110, 670 m, and PS009PC, 552 m).

Considering all data, it appears that in the EM, the climatically "dry" periods since 6 ka are systematically linked to periods of relatively low Nile river runoff, to which *U. peregrina* respond by lowering its abundances, as also discussed in Schmiedl et al. (2010). Yet the presence of the eutrophic *B. marginata* during these "dry" periods (Figure 7) indicates a persistence of high trophic conditions at the seafloor. Dry climatic conditions favor strong wind mixing and dust input, which may enhance the nutrient supply to surface waters and therefore stimulate primary production, similarly to the dry YD interval. Also, dry periods might favor longer spring/summer-type conditions that trigger another type of primary production to which *B. marginata* might respond. Indeed, in the modern Mediterranean, there is a strong seasonal variability in the primary production with an early spring new production dominated by diatoms and a late regenerated production dominated by picoplankton and nanoplankton (e.g., Siokou-Frangou et al., 2010). In the modern Bay of Biscay, *B. marginata* is one of the species that responds only to spring bloom, while *U. peregrina* reacts to the autumnal bloom (Fontanier et al., 2002, 2003; Langezaal et al., 2006). Because they are not mutually exclusive, the combination of the two hypotheses, a lower phytodetritus export and a change in the nature of the primary production during those dry events, might explain the observed faunal pattern.

Superimposed on the *B. marginata*/*U. peregrina* oscillations, *U. mediterranea* record its maximum Holocene values from ~2 to 1 ka (Figure 7a). A similar feature is also recorded in the nearby core SL 112, albeit not discussed (Schmiedl et al., 2010). The EM in general shows an increase in the relative abundance of mesotrophic endobenthic species (Reiss et al., 1999). Note that in our core, the increase in *U. mediterranea*'s abundances is recorded during a time period of relatively low abundance of both *B. marginata*/*U. peregrina* species. As previously discussed for the glacial-deglaciation section, we suggest that *U. mediterranea* traces the

enhancement of the Nile River activity because of its high tolerance to refractory organic matter. The enhancement of terrestrial inputs due to the human activity inducing an increase of erosion in the Nile catchment area at that time (Castañeda et al., 2010) might explain this ecological change. Indeed, since 2–2.5 ka, an increase in the total Nile sediment flux has been reported (Krom et al., 2002), which occurred simultaneously with the falling of lake levels in the Ethiopian highlands (Gasse, 1977; Hassan, 1997) and an increased deforestation (Nyssen et al., 2004). An increase in terrestrial material from 2 ka in the area is supported by (i) the increase of the Ti/Al ratio in PS009PC sediments (Hennekam et al., 2014), (ii) the BIT index from the nearby core GeoB 7702-3 (Castañeda et al., 2010; see Figure S4), and (iii) the sharp increase in the sedimentation rate in cores GA-110 and GA-112 (Schilman, Bar-Matthews, et al., 2001). A high anthropogenic impact would explain an increase in refractory organic matter export to the Levantine Basin without implying an enhancement of the Nile runoff. Also, an increase in riverine nutrient load was suggested to explain the development of planktic opportunistic taxa (e.g., *G. bulloides*) without lowering the planktic species diversity through low salinity during this time period (Mojtahid et al., 2015).

5.3. Changes in the Eastern Mediterranean Overturning Circulation

Planktic and benthic $\delta^{18}O$-$\delta^{13}C$ crossplots can be used to distinguish and isolate specific time intervals and transitions during the last 19 ka (Figure 6). The $\delta^{18}O$-$\delta^{13}C$ clusters were made using PCA analysis (see Figure S2). Although some differences are found in the timing between benthic and planktic crossplots, these periods roughly correspond to the glacial interval, the deglaciation, the Holocene-sapropel event, and the mid-Holocene to Late Holocene (Figure 6).

The decoupling between benthic and planktic $\delta^{18}O$ and $\delta^{13}C$ signatures for the second part of H1 event (~16.5–15 ka) is noteworthy (Figure 6). While the planktic $\delta^{18}O$-$\delta^{13}C$ clusters H1 and LGM isotopic values together, the benthic $\delta^{18}O$-$\delta^{13}C$ separates the two phases of H1, similarly to what has been observed in the benthic foraminiferal assemblage (Figure 7). The $\Delta\delta^{13}C$p-b is negative (benthic $\delta^{13}C$ > planktic $\delta^{13}C$) during this time interval, which is most likely due to relatively high benthic $\delta^{13}C$ values in this second phase of H1 (Figure 6). These high values of benthic $\delta^{13}C$ are not stable over time but show a first increase from 16.5 to 15.7 ka followed by a ~0.7‰ decrease until the mid-B/A event (Figure 5). The same trend, albeit of less amplitude, is found in a nearby record (MD04-2722; Cornuault et al., 2016) and in the EM isotopic compilation of Grimm et al. (2015; Figure 5b). Although these authors do not give an explanation for the first benthic $\delta^{13}C$ increase, we here hypothesize an active production of intermediate water masses (glacial analog of LIW) enriching benthic environments in ^{13}C. For the following decreasing trend in benthic $\delta^{13}C$ from late H1, these authors suggested a progressively sluggish ventilation of the deep sea. The study of Cornuault et al. (2018) use neodymium isotopes in core MD04-2722 further to hypothesize that enhanced EM stratification is associated to a higher contribution of the Modified Atlantic Water. That said, the overall negative $\Delta^{13}C$p-b (benthic $\delta^{13}C$ > planktic $\delta^{13}C$) during the second part of H1 (~16.5–15 ka) is complex and may be the result of both the benthic signature and relatively low values of planktic $\delta^{13}C$ due to either low productivity or inflow of Nile water with low riverine $\delta^{13}C$-DIC values characterizing this period (Figure 5).

The foraminiferal assemblages indicate enhanced productivity during the YD (Figure 8), while the close to zero $\Delta\delta^{13}C$p-b may point towards the opposite. For this time period, a generally good vertical mixing due to wind activity is supported by the presence of deep-dwelling planktic species such as *Globorotalia truncatulinoides* (Mojtahid et al., 2015). Similar benthic community changes as those we found in our record were interpreted as responding to a period of a better ventilation within a general context of sluggish circulation over the AHP (Abu-Zied et al., 2008; Kuhnt et al., 2007; Minto'o et al., 2015), a feature confirmed by modeling (Grimm et al., 2015). An enhanced ventilation of bottom waters would explain the increase of the benthic $\delta^{13}C$, which together with the high values of planktic $\delta^{13}C$ (i.e., high productivity) would explain the close to zero $\Delta\delta^{13}C$p-b.

The S1 event is marked by a large discharge from the Nile River (e.g., Kholeif & Mudie, 2009; Weldeab et al., 2002; Weldeab et al., 2014), clearly indicated in our core by very low planktic $\delta^{18}O$ values (Hennekam et al., 2014). This period is also identified in our planktic $\delta^{18}O$-$\delta^{13}C$ crossplot with $\delta^{18}O$ values lower than the post-S1/Holocene $\delta^{18}O$ values (Figure 6).

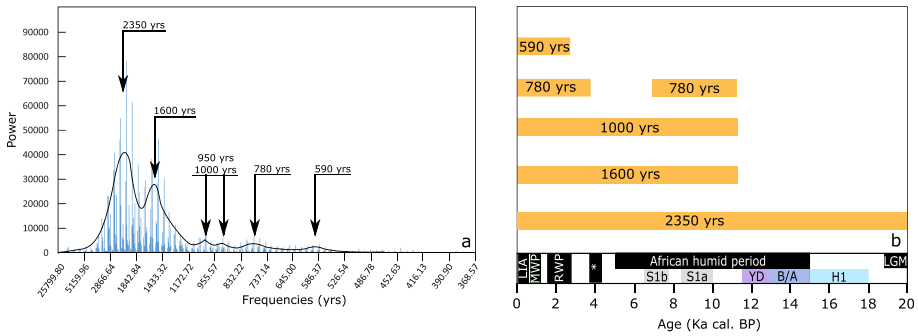

Figure 9. Temporal frequencies of benthic relative abundances in core PS009PC. (a) The presented frequencies are obtained from all REDFIT analyses performed on the dominant species and mean abundance spectrum of the glacial and Holocene groups (see Figure 2). The plain line represents 3-point smooth line. The frequencies of the peaks are extracted from the smoothed line. (b) The temporal occurrence of the frequencies is reported schematically along the record. The detailed REDFIT and wavelet analyses for each species are reported in Figure S5.

From both the benthic and planktic data, the $\delta^{18}O$-$\delta^{13}C$ clusters encompassing the S1 event start 500 to 800 years before the onset (at ~10.1 ka) of sapropel S1 at this core location and depth (Hennekam et al., 2014). This suggests a change in the water column stable isotopic composition before the deposition of the organic-rich sapropel layer. This time lag has been reported before in the EM literature (e.g., Grimm et al., 2015; Revel et al., 2014; Weldeab et al., 2014), although the timing is not always agreed upon as it can take a couple of hundreds or even thousands of years to get a water column (or at least sediment pore space) completely devoid of oxygen. Hereafter, we refer to these two clusters (benthic and planktic) as "S1-like," because they also include that interval before the deposition of S1 at this core location.

Both planktic and benthic $\delta^{18}O$-$\delta^{13}C$ crossplots subdivided the "S1-like" cluster into two groups: Group (i) including pre-S1a and S1a and Group (ii) including the S1 interruption and S1b (Figure 5). However, two main differences exist between the planktic and benthic data. Firstly, the benthic $\delta^{18}O$ values for the whole "S1-like" period are systematically higher than the Holocene $\delta^{18}O$ benthic values, whereas the opposite is observed for the planktic $\delta^{18}O$ (i.e., large $\Delta\delta^{18}$Op-b; Figure 6). Secondly, the lowest benthic $\delta^{18}O$ and $\delta^{13}C$ values are recorded for Group (ii), whereas the opposite is found for the planktic $\delta^{18}O$ and $\delta^{13}C$ (Figures 6b and 6c). The strong water column stratification characterizing S1 (e.g., Casford et al., 2003; Cornuault et al., 2018; Emeis et al., 2000; Mangini & Schlosser, 1986; Rohling et al., 2015), by creating a strong and shallow halocline, may have prevented the mixing between surface and deep waters, explaining therefore the large $\Delta\delta^{18}$Op-b values of the Group (i; Figure 6). However, the studies of Rohling (1994) and Myers et al. (1998), using a general circulation model, and more recently Mojtahid et al. (2019), using benthic foraminiferal Na/Ca from the same PS009PC core, have shown a reduction in salinity at 450- to 550-m water depth during S1. If this salinity drop is not directly due to low-saline surface waters, it might be linked to the presence of a different water mass bathing the study area during S1. Rohling (1994) hypothesized the presence of stagnant less saline old deep water (~37.4 PSU) remaining after the deglaciation below 400–450 m in the Levantine Basin, at least during the most anoxic part of S1 (i.e., S1a). As such, a stagnant old deep water will decrease the $\delta^{13}C$ signature of the benthic foraminifera. This hypothesis might also explain the significant offset observed in the difference between the benthic and planktic $\delta^{13}C$ signature ($\Delta\delta^{13}$Cp-b, Figure 7c).

Paradoxically, while the old deep water would be mainly present at S1a, the $\Delta\delta^{13}$Cp-b offset is maximal for Group (ii) encompassing the S1b ($\Delta\delta^{13}$Cp-b = 0.8‰, Figure 7c). Under higher productivity environments with low dissolved oxygen and sedimentary carbonate content, such as during S1a, the isotopic composition of DIC in seawater decreases as the pH increases due to carbonate speciation (Zeebe et al., 1999). This effect known as the carbonate ion undersaturation effect (Lea et al., 1999; Mackensen, 2008; Mackensen & Licari, 2004) counterbalances the trophic/circulation effect, increasing therefore the benthic isotopic signature and thus might explain a lower $\Delta\delta^{13}$Cp-b values for Group (i). That said, this period should be interpreted with care, if only for the low numbers of benthic isotopic measurements (Figure 5).

After the sapropel S1 (since ~6.5 ka), both planktic and benthic $\delta^{18}O$-$\delta^{13}C$ crossplots indicate a rather stable isotopic signal. This probably suggests that the EM vertical water mass distribution, after recovering from the S1 event, is most likely similar to the modern configuration.

5.4. Foraminiferal Response to Long- and Short-Timescale Forcing Processes

Climatic and environmental conditions over the past 19 ka in the EM are known to be affected by both orbital and suborbital forcing mechanisms (e.g., Hamann et al., 2009; Hennekam et al., 2014; Mojtahid et al., 2015; Revel et al., 2014; Schmiedl et al., 2010). In our record, the long-timescale trend linked to the orbital-forced glacial-interglacial transition is well recorded in both our benthic and planktic foraminiferal $\delta^{18}O$ records (Figure 5a). On this long-term trend is superimposed shorter timescale $\delta^{18}O$ variability, matching known climatic periods such as H1, B/A, and YD events across the last deglaciation (Figure 5a).

The observed variability in the planktic foraminiferal records was also investigated through spectral analyses (Hennekam et al., 2014) and multicentennial variability at around 500 and 1,000 years were linked to solar forcing, as those frequencies are similar to the variability in atmospheric $\Delta^{14}C_{res}$ (Stuiver et al., 1998). For purpose of comparison, we conducted similar spectral analyses on the benthic relative abundances obtained in this study (Figure 9). Those two frequencies were also detected in the benthic records. We further record the 2400-year solar mode well known in Atlantic paleoclimatic records throughout the Holocene (e.g., Dansgaard et al., 1984; O'Brien et al., 1995) as the Hallstatt cycle (Dergachev & Chistyakov, 1995; Hood & Jirikowic, 1990; Hoyt & Schatten, 1997; Scafetta et al., 2016). This solar mode is also reported in the EM, from the planktic-based reconstructed sea surface temperatures of the Aegean Sea (Rohling, Mayewsk, et al., 2002). Interestingly, the conducted benthic spectral analyses detected a supplementary frequency at around 1,660 years to which the 800-year mode might be the secondary harmonic. To our knowledge, this mode was never reported in the Mediterranean Sea. However, the ~1,600-year spectral signature is widely recorded in the Holocene in Atlantic paleoclimatic records (deMenocal, Ortiz, Guilderson, Adkins, et al., 2000, deMenocal, Ortiz, Guilderson, & Sarnthein, 2000; McDermott et al., 2001; Moros et al., 2004). The solar forcing was previously argued to explain this periodicity (Bond et al., 2001) but is now largely debated (Debret et al., 2007; Dima & Lohmann, 2009; Soon et al., 2014). The 1,600-year periodicity is now attributed to an internal forcing, at least for the Late Holocene, likely oceanic-driven as suggested by Broecker et al. (1999) and McManus et al. (1999) and resulting from the thermohaline sensitivity to the north European meltwater discharge (Debret et al., 2009). Either the reported 1,600-year periodicity from our benthic records is linked to the Atlantic circulation mode or results from an internal Mediterranean circulation mode cannot be deciphered here. Because spectral analyses conducted on foraminiferal data are very sparse in the Mediterranean Sea, we highly recommend a more extensive use for such analytical approach to investigate more accurately the forcing processes that might control this 1,600-year periodicity.

6. Conclusions

Our benthic foraminiferal and stable isotope records from the EM PS009PC core suggest a strong response of the communities to the food flux since 19 ka, which in turn is sensitively linked to climate forcing. During the last deglaciation (19 to 10 ka), the nutrient flux is conditioned by the Nile River inputs and therefore by the intensity of the African monsoon, leading to changes in the trophic conditions in the Levantine Basin. The coupling with planktic data indicates that the period extending from the end of the LGM until the mid-H1 event (~16.5 ka) is characterized by a good vertical mixing leading to high trophic conditions at the sea bottom. From the second phase of H1 event until the start of S1, the productivity generally decreases and the overturning circulation progressively weakens with the exception of the Younger Dryas (~12.8 to 11.5 ka).

During S1 (~10.1 to 6.5 ka), both benthic and planktic communities strongly respond to the increase of the Nile River activity. While the planktic foraminifera indicate increased primary production together with increased terrestrial carbon input, the benthic community records the decrease in oxygen content at the bottom. The coupled benthic-planktic carbon stable isotope signature indicates an overall poor ventilation of bottom waters with a likely presence of old deep-water masses bathing the bottom layers of a highly stratified water column. In addition, our data indicate a change in the stable carbon and oxygen isotopic composition of the water column ~0.5–0.8 ka prior to the deposition of the organic-rich sapropel layer, which suggests

that it can take a couple of hundreds of years, at this depth and location, to get the bottom environment depleted in oxygen.

During the Holocene, the trophic conditions remain relatively high with no evidence of strong modulation by the Nile River activity. Yet the benthic community show strong changes. These changes are punctuated mainly by the alternating presence of the eutrophic species *B. marginata* and *U. peregrina* in relation to dry/humid climatic oscillations since the last 6 ka. We hypothesize that the dry/humid climatic oscillations influence the nature of primary producers to which those species respond. The high occurrence of *B. marginata* (in opposite to *U. peregrina*) matches three climatically dry periods (the "4.2-ka event" and the RWP and MWP time periods), during which the nature of primary production may have been favored by wind mixing and dust input, similarly to the YD. However, an enhancement of the Nile River sediment input to the Levantine Basin was recorded at around 2 ka and interpreted as the result of increased anthropogenic activity in the region encompassing the Nile catchment area leading to higher erosion rate, rather than to an enhancement of the Nile River activity.

The analysis of the embedded periodicities in the benthic relative abundance records highlights the presence of a strong solar frequencies (~1,000- and 500-year cycles), as previously found from the planktic data. However, a supplementary ~1600-year mode was found in the benthic records. The absence of the latter frequency in the planktic data may indicate an overturning circulation-driven forcing of this cycle.

Acknowledgments
This study was carried out in the context of collaboration between the University of Angers and the University of Utrecht. This study was funded by the international program MISTRALS PaleoMEX under the project MADHO (MediterraneAn Deltas in the Holocene) and by France's Regional Council of Pays de la Loire (under the TANDEM project). The Netherlands Organisation for Scientific Research (now) is acknowledged for financial support to the PASSAP cruise and the PALM project (820.01.005). Data used for this paper can be found using the Mendeley data repository (DOI: 10.17632/4s4f744t24.2). We warmly thank Editor-in-Chief Ellen Thomas, reviewer Gerhard Schmiedl, and the two anonymous reviewers for their thorough reviews and very helpful comments that improved the initial version of the manuscript.

References

Abu-Zied, R. H., Rohling, E. J., Jorissen, F. J., Fontanier, C., Casford, J. S. L., & Cooke, S. (2008). Benthic foraminiferal response to changes in bottom-water oxygenation and organic carbon flux in the eastern Mediterranean during LGM to recent times. *Marine Micropaleontology*, *67*(1), 46–68. https://doi.org/10.1016/j.marmicro.2007.08.006

Adamson, D. A., Gasse, F., Street, F. A., & Williams, M. A. J. (1980). Late Quaternary history of the Nile. *Nature*, *288*, 50–55.

Adloff, F., Somot, S., Sevault, F., Jordà, G., Aznar, R., Déqué, M., et al. (2015). Mediterranean Sea response to climate change in an ensemble of twenty first century scenarios. *Climate Dynamics*, *45*(9-10), 2775–2802. https://doi.org/10.1007/s00382-015-2507-3

Almogi-Labin, A., Bar-Matthews, M., Shriki, D., Kolosovsky, E., Paterne, M., Schilman, B., et al. (2009). Climatic variability during the last ~90 ka of the southern and northern Levantine Basin as evident from marine records and speleothems. *Quaternary Science Reviews*, *28* (25-26), 2882–2896. https://doi.org/10.1016/j.quascirev.2009.07.017

Altenbach, A. V., Pflaumann, U., Schiebel, R., Thies, A., Timm, S., & Trauth, M. (1999). Scaling percentages and distributional patterns of benthic foraminifera with flux rates of organic carbon. *The Journal of Foraminiferal Research*, *29*(3), 173–185.

Avnaim-Katav, S., Almogi-Labin, A., Schneider-Mor, A., Crouvi, O., Burke, A. A., Kremenetski, K. V., & MacDonald, G. M. (2019). A multi-proxy shallow marine record for Mid-to-Late Holocene climate variability, Thera eruptions and cultural change in the Eastern Mediterranean. *Quaternary Science Reviews*, *204*, 133–148. https://doi.org/10.1016/j.quascirev.2018.12.001

Bar-Matthews, M., Ayalon, A., Gilmour, M., Matthews, A., & Hawkesworth, C. J. (2003). Sea–land oxygen isotopic relationships from planktonic foraminifera and speleothems in the Eastern Mediterranean region and their implication for paleorainfall during interglacial intervals. *Geochimica et Cosmochimica Acta*, *67*(17), 3181–3199. https://doi.org/10.1016/S0016-7037(02)01031-1

Bar-Matthews, M., Ayalon, A., & Kaufman, A. (1997). Late Quaternary paleoclimate in the eastern Mediterranean region from stable isotope analysis of speleothems at Soreq Cave, Israel. *Quaternary Research*, *47*(2), 155–168. https://doi.org/10.1006/qres.1997.1883

Bar-Matthews, M., Ayalon, A., Kaufman, A., & Wasserburg, G. J. (1999). The eastern Mediterranean paleoclimate as a reflection of regional events: Soreq Cave, Israel. *Earth and Planetary Science Letters*, *166*(1), 85–95. https://doi.org/10.1016/S0012-821X(98)00275-1

Bartov, Y., Goldstein, S. L., Stein, M., & Enzel, Y. (2003). Catastrophic arid episodes in the Eastern Mediterranean linked with the North Atlantic Heinrich events. *Geology*, *31*(5), 439–442. https://doi.org/10.1130/0091-7613(2003)031<0439:CAEITE>2.0.CO;2

Berger, A., & Loutre, M. F. (1991). Insolation values for the climate of the last 10 million years. *Quaternary Science Reviews*, *10*(4), 297–317. https://doi.org/10.1016/0277-3791(91)90033-Q

Bolle, H.-J. (Ed) (2003). *Mediterranean climate: Variability and trends*. Berlin Heidelberg: Springer-Verlag. Retrieved from. https://www.springer.com/fr/book/9783642628627

Bond, G., Kromer, B., Beer, J., Muscheler, R., Evans, M., Showers, W., et al. (2001). Persistent solar influence on North Atlantic climate during the Holocene. *Science*, *294*(5549), 2130–2136. https://doi.org/10.1126/science.1065680

Bout-Roumazeilles, V., Combourieu Nebout, N., Peyron, O., Cortijo, E., Landais, A., & Masson-Delmotte, V. (2007). Connection between South Mediterranean climate and North African atmospheric circulation during the last 50,000 yr BP North Atlantic cold events. *Quaternary Science Reviews*, *26*(25), 3197–3215. https://doi.org/10.1016/j.quascirev.2007.07.015

Box, M. R., Krom, M. D., Cliff, R., Almogi-Labin, A., Bar-Matthews, M., Ayalon, A., et al. (2008). Changes in the flux of Saharan dust to the East Mediterranean Sea since the last glacial maximum as observed through Sr-isotope geochemistry. *Mineralogical Magazine*, *72*(1), 307–311. https://doi.org/10.1180/minmag.2008.072.1.307

Box, M. R., Krom, M. D., Cliff, R., Bar-Matthews, M., Almogi-Labin, A., Ayalon, A., & Paterne, M. (2011). Response of the Nile and its catchment to millennial-scale climatic change since the LGM from Sr isotopes and major elements of East Mediterranean sediments. *Quaternary Science Reviews*, *30*(3-4), 431–442. https://doi.org/10.1016/j.quascirev.2010.12.005

Broecker, W. S., Sutherland, S., & Peng, T.-H. (1999). A possible 20th-century slowdown of Southern Ocean deep water formation. *Science*, *286*(5442), 1132–1135. https://doi.org/10.1126/science.286.5442.1132

Cacho, I., Grimalt, J. O., Canals, M., Sbaffi, L., Shackleton, N. J., Schönfeld, J., & Zahn, R. (2001). Variability of the western Mediterranean Sea surface temperature during the last 25,000 years and its connection with the Northern Hemisphere climatic changes. *Paleoceanography*, *16*(1), 40–52. https://doi.org/10.1029/2000PA000502

Cacho, I., Grimalt, J. O., Pelejero, C., Canals, M., Sierro, F. J., Flores, J. A., & Shackleton, N. (1999). Dansgaard-Oeschger and Heinrich event imprints in Alboran Sea paleotemperatures. *Paleoceanography*, *14*(6), 698–705. https://doi.org/10.1029/1999PA900044

Casford, J. S. L., Rohling, E. J., Abu-Zied, R., Cooke, S., Fontanier, C., Leng, M., & Lykousis, V. (2002). Circulation changes and nutrient concentrations in the late Quaternary Aegean Sea: A nonsteady state concept for sapropel formation. *Paleoceanography*, *17*(2), 1024. https://doi.org/10.1029/2000PA000601

Casford, J. S. L., Rohling, E. J., Abu-Zied, R. H., Fontanier, C., Jorissen, F. J., Leng, M. J., et al. (2003). A dynamic concept for eastern Mediterranean circulation and oxygenation during sapropel formation. *Palaeogeography, Palaeoclimatology, Palaeoecology*, *190*, 103–119. https://doi.org/10.1016/S0031-0182(02)00601-6

Castañeda, I. S., Schefuß, E., Pätzold, J., Sinninghe Damsté, J. S., Weldeab, S., & Schouten, S. (2010). Millennial-scale sea surface temperature changes in the eastern Mediterranean (Nile River Delta region) over the last 27,000 years. *Paleoceanography*, *25*(1), PA1208. https://doi.org/10.1029/2009PA001740

Cornuault, M., Tachikawa, K., Vidal, L., Guihou, A., Siani, G., Deschamps, P., et al. (2018). Circulation changes in the eastern Mediterranean Sea over the past 23,000 years inferred from authigenic Nd isotopic ratios. *Paleoceanography and Paleoclimatology*, *33*(3), 264–280. https://doi.org/10.1002/2017PA003227

Cornuault, M., Vidal, L., Tachikawa, K., Licari, L., Rouaud, G., Sonzogni, C., & Revel, M. (2016). Deep water circulation within the eastern Mediterranean Sea over the last 95 kyr: New insights from stable isotopes and benthic foraminifera assemblages. *Palaeogeography, Palaeoclimatology, Palaeoecology*, *459*, 1–14. https://doi.org/10.1016/j.palaeo.2016.06.038

Cullen, H. M., deMenocal, P. B., Hemming, S., Hemming, G., Brown, F. H., Guilderson, T., & Sirocko, F. (2000). Climate change and the collapse of the Akkadian empire: Evidence from the deep sea. *Geology*, *28*(4), 379–382. https://doi.org/10.1130/0091-7613(2000)28<379:CCATCO>2.0.CO;2

Cullen, J. L. (1981). Microfossil evidence for changing salinity patterns in the Bay of Bengal over the last 20 000 years. *Palaeogeography, Palaeoclimatology, Palaeoecology*, *35*, 315–356. https://doi.org/10.1016/0031-0182(81)90101-2

Dansgaard, W., Johnsen, S., Clausen, H., Dahl-Jensen, D., Gundestrup, N., Hammer, C., & Oeschger, H. (1984). North Atlantic climatic oscillations revealed by deep Greenland ice cores. In J. E. Hansen & T. Takahashi (Eds.), *Climate processes and climate sensitivity*, *Geophysical Monograph Series* (Chap. 5, Vol. 29, pp. 288–298). American Geophysical Union. https://doi.org/10.1029/GM029p0288

De Lange, G. J., Thomson, J., Reitz, A., Slomp, C. P., Speranza Principato, M., Erba, E., & Corselli, C. (2008). Synchronous basin-wide formation and redox-controlled preservation of a Mediterranean sapropel. *Nature Geoscience*, *1*(9), 606–610. https://doi.org/10.1038/ngeo283

De Rijk, S., Hayes, A., & Rohling, E. J. (1999). Eastern Mediterranean sapropel S1 interruption: An expression of the onset of climatic deterioration around 7 ka BP. *Marine Geology*, *153*(1), 337–343. https://doi.org/10.1016/S0025-3227(98)00075-9

De Rijk, S., Jorissen, F. J., Rohling, E. J., & Troelstra, S. R. (2000). Organic flux control on bathymetric zonation of Mediterranean benthic foraminifera. *Marine Micropaleontology*, *40*(3), 151–166. https://doi.org/10.1016/S0377-8398(00)00037-2

Debret, M., Bout-Roumazeilles, V., Grousset, F., Desmet, M., Mcmanus, J. F., Massei, N., et al. (2007). The origin of the 1500-year climate cycles in Holocene North-Atlantic records. *Climate of the Past Discussions*, *3*(2), 679–692. https://doi.org/10.5194/cpd-3-679-2007

Debret, M., Sebag, D., Costra, X., Massei, N., Petit, J. R., Chapron, E., & Bout-Roumazeilles, V. (2009). Evidence from wavelet analysis for a mid-Holocene transition in global climate forcing. *Quaternary Science Reviews*, *28*(25–26), 2675–2688. https://doi.org/10.1016/j.quascirev.2009.06.005

deMenocal, P., Ortiz, J., Guilderson, T., Adkins, J., Sarnthein, M., Baker, L., & Yarusinsky, M. (2000). Abrupt onset and termination of the African Humid Period: Rapid climate responses to gradual insolation forcing. *Quaternary Science Reviews*, *19*(1), 347–361. https://doi.org/10.1016/S0277-3791(99)00081-5

deMenocal, P., Ortiz, J., Guilderson, T., & Sarnthein, M. (2000). Coherent high- and low-latitude climate variability during the Holocene Warm Period. *Science*, *288*(5474), 2198–2202. https://doi.org/10.1126/science.288.5474.2198

Denton, G. H., Anderson, R. F., Toggweiler, J. R., Edwards, R. L., Schaefer, J. M., & Putnam, A. E. (2010). The last glacial termination. *Science*, *328*(5986), 1652–1656. https://doi.org/10.1126/science.1184119

Dergachev, V., & Chistyakov, V. (1995). Cosmogenic radiocarbon and cyclical natural processes. *Geology*, *37*(2), 417–424. https://doi.org/10.1017/S0033822200030897

Dima, M., & Lohmann, G. (2009). Conceptual model for millennial climate variability: A possible combined solar-thermohaline circulation origin for the ~1500-year cycle. *Climate Dynamics*, *32*, 301–311. https://doi.org/10.1007/s00382-008-0471-x

Dixit, Y., Hodell, D. A., & Petrie, C. A. (2014). Abrupt weakening of the summer monsoon in northwest India ~4100 yr ago. *Geology*, *42*(4), 339–342. https://doi.org/10.1130/G35236.1

Dormoy, I., Peyron, O., Combourieu-Nebout, N., Goring, S., Kotthoff, U., Magny, M., & Pross, J. (2009). Terrestrial climate variability and seasonality changes in the Mediterranean region between 15 000 and 4 000 years BP deduced from marine pollen records. *Climate of the Past*, *5*, 615–632.

Drinia, H., Antonarakou, A., Tsourou, T., Kontakiotis, G., Psychogiou, M., & Anastasakis, G. (2016). Foraminifera eco-biostratigraphy of the southern Evoikos outer shelf, central Aegean Sea, during MIS 5 to present. *Continental Shelf Research*, *126*, 36–49. https://doi.org/10.1016/j.csr.2016.07.009

Ehrmann, W., Schmiedl, G., Hamann, Y., Kuhnt, T., Hemleben, C., & Siebel, W. (2007). Clay minerals in late glacial and Holocene sediments of the northern and southern Aegean Sea. *Palaeogeography, Palaeoclimatology, Palaeoecology*, *249*(1), 36–57. https://doi.org/10.1016/j.palaeo.2007.01.004

Emeis, K., Struck, U., Schulz, H.-M., Rosenberg, R., Bernasconi, S., Erlenkeuser, H., et al. (2000). Temperature and salinity variations of Mediterranean Sea surface waters over the last 16,000 years from records of planktonic stable oxygen isotopes and alkenone unsaturation ratios. *Palaeogeography, Palaeoclimatology, Palaeoecology*, *158*(3-4), 259–280. https://doi.org/10.1016/S0031-0182(00)00053-5

Essallami, L., Sicre, M. A., Kallel, N., Labeyrie, L., & Siani, G. (2007). Hydrological changes in the Mediterranean Sea over the last 30,000 years. *Geochemistry, Geophysics, Geosystems*, *8*(7), Q07002. https://doi.org/10.1029/2007GC001587

Evans, J. P., Smith, R. B., & Oglesby, R. J. (2004). Middle East climate simulation and dominant precipitation processes. *International Journal of Climatology*, *24*(13), 1671–1694. https://doi.org/10.1002/joc.1084

Flaux, C., El-Assal, M., Marriner, N., Morhange, C., Rouchy, J.-M., Soulié-Märsche, I., & Torab, M. (2012). Environmental changes in the Maryut lagoon (northwestern Nile delta) during the last ~2000 years. *Journal of Archaeological Science*, *39*(12), 3493–3504. https://doi.org/10.1016/j.jas.2012.06.010

Fleitmann, D., Burns, S. J., Mangini, A., Mudelsee, M., Kramers, J., Villa, I., et al. (2007). Holocene ITCZ and Indian monsoon dynamics recorded in stalagmites from Oman and Yemen (Socotra). *Quaternary Science Reviews*, *26*(1-2), 170–188. https://doi.org/10.1016/j.quascirev.2006.04.012

Fleming, K., Johnston, P., Zwartz, D., Yokoyama, Y., Lambeck, K., & Chappell, J. (1998). Refining the eustatic sea-level curve since the Last Glacial Maximum using far- and intermediate-field sites. *Earth and Planetary Science Letters*, *163*(1), 327–342. https://doi.org/10.1016/S0012-821X(98)00198-8

Fontanier, C., Jorissen, F. J., Chaillou, G., David, C., Anschutz, P., & Lafon, V. (2003). Seasonal and interannual variability of benthic foraminiferal faunas at 550 m depth in the Bay of Biscay. *Deep Sea Research Part I: Oceanographic Research Papers*, *50*(4), 457–494. https://doi.org/10.1016/S0967-0637(02)00167-X

Fontanier, C., Jorissen, F. J., Lansard, B., Mouret, A., Buscail, R., Schmidt, S., et al. (2008). Live foraminifera from the open slope between Grand Rhône and Petit Rhône Canyons (Gulf of Lions, NW Mediterranean). *Deep Sea Research Part I: Oceanographic Research Papers*, *55*(11), 1532–1553. https://doi.org/10.1016/j.dsr.2008.07.003

Fontanier, C., Jorissen, F. J., Licari, L., Alexandre, A., Anschutz, P., & Carbonel, P. (2002). Live benthic foraminiferal faunas from the Bay of Biscay: Faunal density, composition, and microhabitats. *Deep Sea Research Part I: Oceanographic Research Papers*, *49*(4), 751–785. https://doi.org/10.1016/S0967-0637(01)00078-4

Fontanier, C., Mackensen, A., Jorissen, F. J., Anschutz, P., Licari, L., & Griveaud, C. (2006). Stable oxygen and carbon isotopes of live benthic foraminifera from the Bay of Biscay: Microhabitat impact and seasonal variability. *Marine Micropaleontology*, *58*(3), 159–183. https://doi.org/10.1016/j.marmicro.2005.09.004

Freydier, R., Michard, A., De Lange, G., & Thomson, J. (2001). Nd isotopic compositions of Eastern Mediterranean sediments: Tracers of the Nile influence during sapropel S1 formation? *Marine Geology*, *177*(1), 45–62. https://doi.org/10.1016/S0025-3227(01)00123-2

Frumkin, A., Magaritz, M., Carmi, I., & Zak, I. (1991). The Holocene climatic record of the salt caves of Mount Sedom Israel. *The Holocene*, *1*(3), 191–200. https://doi.org/10.1177/095968369100100301

Gasse, F. (1977). Evolution of Lake Abhé (Ethiopia and TFAI), from 70,000 b.p. *Nature*, *265*(5589), 42–45. https://doi.org/10.1038/265042a0

Gasse, F., Vidal, L., Develle, A.-L., & Campo, E. V. (2011). Hydrological variability in the Northern Levant: A 250 ka multi-proxy record from the Yammoûneh (Lebanon) sedimentary sequence. *Climate of the Past*, *7*(4), 1261–1284. https://doi.org/10.5194/cp-7-1261-2011

Geraga, M., Mylona, G., Tsaila-Monopoli, S., Papatheodorou, G., & Ferentinos, G. (2008). Northeastern Ionian Sea: Palaeoceanographic variability over the last 22 ka. *Journal of Marine Systems*, *74*(1), 623–638. https://doi.org/10.1016/j.jmarsys.2008.05.019

Giamali, C., Koskeridou, E., Antonarakou, A., Ioakim, C., Kontakiotis, G., Karageorgis, A. P., et al. (2019). Multiproxy ecosystem response of abrupt Holocene climatic changes in the northeastern Mediterranean sedimentary archive and hydrologic regime. *Quaternary Research*, *92*(3), 665–685. https://doi.org/10.1017/qua.2019.38

Giorgi, F. (2006). Climate change hot-spots. *Geophysical Research Letters*, *33*(8), L08707. https://doi.org/10.1029/2006GL025734

Giorgi, F., & Lionello, P. (2008). Climate change projections for the Mediterranean region. *Global and Planetary Change*, *63*(2-3). https://doi.org/10.1016/j.gloplacha.2007.09.005

Giunta, S., Negri, A., Morigi, C., Capotondi, L., Combourieu-Nebout, N., Emeis, K. C., et al. (2003). Coccolithophorid ecostratigraphy and multi-proxy paleoceanographic reconstruction in the Southern Adriatic Sea during the last deglacial time (core AD91-17). *Palaeogeography, Palaeoclimatology, Palaeoecology*, *190*, 39–59. https://doi.org/10.1016/S0031-0182(02)00598-9

Grimm, R., Maier-Reimer, E., Mikolajewicz, U., Schmiedl, G., Müller-Navarra, K., Adloff, F., et al. (2015). Late glacial initiation of Holocene eastern Mediterranean sapropel formation. *Nature Communications*, *6*(1), 1, 7099–12. https://doi.org/10.1038/ncomms8099

Hamann, Y., Ehrmann, W., Schmiedl, G., & Kuhnt, T. (2009). Modern and late Quaternary clay mineral distribution in the area of the SE Mediterranean Sea. *Quaternary Research*, *71*, 453–464. https://doi.org/10.1016/j.yqres.2009.01.001

Hammer, Ø., Harper, D. A. T., Ryan, P., & D. (2001). PAST: Paleontological statistics software package for education and data analysis. *Palaeontologia Electronica*, *4*(1), 9.

Hassan, F. A. (1997). Holocene palaeoclimates of Africa. *African Archaeological Review*, *14*(4), 213–230. https://doi.org/10.1023/A:1022255800388

Hennekam, R., & de Lange, G. (2012). X-ray fluorescence core scanning of wet marine sediments: Methods to improve quality and reproducibility of high-resolution paleoenvironmental records. *Limnology and Oceanography: Methods*, *10*(12), 991–1003. https://doi.org/doi:10.4319/lom.2012.10.991

Hennekam, R., Donders, T. H., Zwiep, K., & de Lange, G. J. (2015). Integral view of Holocene precipitation and vegetation changes in the Nile catchment area as inferred from its delta sediments. *Quaternary Science Reviews*, *130*, 189–199. https://doi.org/10.1016/j.quascirev.2015.05.031

Hennekam, R., Jilbert, T., Schnetger, B., & de Lange, G. J. (2014). Solar forcing of Nile discharge and sapropel S1 formation in the early to middle Holocene eastern Mediterranean. *Paleoceanography*, *29*(5), 343–356. https://doi.org/10.1002/2013PA002553

Herguera, J. C., & Berger, W. H. (1991). Paleoproductivity from benthic foraminifera abundance: Glacial to postglacial change in the west-equatorial Pacific. *Geology*, *19*(12), 1173–1176. https://doi.org/10.1130/0091-7613(1991)019<1173:PFBFAG>2.3.CO;2

Hoegh-Guldberg, O., Jacob, D., Taylor, M., Bindi, M., Brown, S., Camilloni, I., et al. (2018). Impacts of 1.5 °C of global warming on natural and human systems. In V. Masson-Delmotte et al. (Eds.), *Global Warming of 1.5°C. An IPCC Special Report on the impacts of global warming of 1.5°C above pre-industrial levels and related global greenhouse gas emission pathways, in the context of strengthening the global response to the threat of climate change* (Chap. 3, pp. 175–311). Geneva, Switzerland: World Meteorological Organization Technical Document. Retrieved from https://www.ipcc.ch/sr15/chapter/chapter-3/

Hood, L. L., & Jirikowic, J. L. (1990). Recurring variations of probable solar origin in the atmospheric $\Delta^{14}C$ time record. *Geophysical Research Letters*, *17*(1), 85–88. https://doi.org/10.1029/GL017i001p00085

Hoyt, D. V., & Schatten, K. H. (1997). *The role of the Sun in the climate change*. New York: Oxford Univ Press.

Hyams-Kaphzan, O., Lubinevsky, H., Crouvi, O., Harlavan, Y., Herut, B., Kanari, M., et al. (2018). Live and dead deep-sea benthic foraminiferal macrofauna of the Levantine basin (SE Mediterranean) and their ecological characteristics. *Deep Sea Research Part I: Oceanographic Research Papers*, *136*, 72–83. https://doi.org/10.1016/j.dsr.2018.04.004

Incarbona, A., Abu-Zied, R. H., Rohling, E. J., & Ziveri, P. (2019). Reventilation episodes during the sapropel S1 deposition in the eastern Mediterranean based on holococcolith preservation. *Paleoceanography and Paleoclimatology*, *34*(10), 1597–1609. https://doi.org/10.1029/2019PA003626

Issar, A. S., & Zohar, M. (2004). *Climate change—Environment and civilization in the Middle East*. Berlin Heidelberg: Springer-Verlag. Retrieved from. https://www.springer.com/gp/book/9783662062647

Jorissen, F. J. (1999). Benthic foraminiferal successions across Late Quaternary Mediterranean sapropels. *Marine Geology*, *153*(1), 91–101. https://doi.org/10.1016/S0025-3227(98)00088-7

Kallel, N., Paterne, M., Duplessy, J., Vergnaudgrazzini, C., Pujol, C., Labeyrie, L., et al. (1997). Enhanced rainfall in the Mediterranean region during the last sapropel event. *Oceanolica Acta*, *20*(5), 697–712.

Kaniewski, D., Van Campo, E., Paulissen, E., Weiss, H., Bakker, J., Rossignol, I., & Van Lerberghe, K. (2011). The medieval climate anomaly and the little Ice Age in coastal Syria inferred from pollen-derived palaeoclimatic patterns. *Global and Planetary Change*, *78*(3), 178–187. https://doi.org/10.1016/j.gloplacha.2011.06.010

Kholeif, S. E. A., & Mudie, P. J. (2009). Palynological records of climate and oceanic conditions in the late Pleistocene and Holocene of the Nile Cone, southeastern Mediterranean, Egypt. *Palynology*, *33*(1), 1–24. https://doi.org/10.1080/01916122.2009.9989664

Koho, K. A., García, R., de Stigter, H. C., Epping, E., Koning, E., Kouwenhoven, T. J., & van der Zwaan, G. J. (2008). Sedimentary labile organic carbon and pore water redox control on species distribution of benthic foraminifera: A case study from Lisbon–Setúbal Canyon (southern Portugal). *Progress in Oceanography*, *79*(1), 55–82. https://doi.org/10.1016/j.pocean.2008.07.004

Kontakiotis, G. (2016). Late Quaternary paleoenvironmental reconstruction and paleoclimatic implications of the Aegean Sea (eastern Mediterranean) based on paleoceanographic indexes and stable isotopes. *Quaternary International*, *401*, 28–42. https://doi.org/10.1016/j.quaint.2015.07.039

Kontakiotis, G., Antonarakou, A., & Zachariasse, W. J. (2016). Late Quaternary palaeoenvironmental changes in the Aegean Sea: Interrelations and interactions between North and South Aegean Sea. *Bulletin of the Geological Society of Greece*, *47*(1), 167. https://doi.org/10.12681/bgsg.10920

Kotthoff, U., Pross, J., Müller, U. C., Peyron, O., Schmiedl, G., Schulz, H., & Bordon, A. (2008). Climate dynamics in the borderlands of the Aegean Sea during formation of sapropel S1 deduced from a marine pollen record. *Quaternary Science Reviews*, *27*(7-8), 832–845. https://doi.org/10.1016/j.quascirev.2007.12.001

Krom, M. D., Cliff, R. A., Eijsink, L. M., Herut, B., & Chester, R. (1999). The characterisation of Saharan dusts and Nile particulate matter in surface sediments from the Levantine basin using Sr isotopes. *Marine Geology*, *155*(3), 319–330. https://doi.org/10.1016/S0025-3227(98)00130-3

Krom, M. D., Stanley, J. D., Cliff, R. A., & Woodward, J. C. (2002). Nile River sediment fluctuations over the past 7000 yr and their key role in sapropel development. *Geology*, *30*(1), 71–74. https://doi.org/10.1130/0091-7613(2002)030<0071:NRSFOT>2.0.CO;2

Kuhnt, T., Schmiedl, G., Ehrmann, W., Hamann, Y., & Andersen, N. (2008). Stable isotope composition of Holocene benthic foraminifers from the Eastern Mediterranean Sea: Past changes in productivity and deep water oxygenation. *Palaeogeography, Palaeoclimatology, Palaeoecology*, *268*(1-2), 106–115. https://doi.org/10.1016/j.palaeo.2008.07.010

Kuhnt, T., Schmiedl, G., Ehrmann, W., Hamann, Y., & Hemleben, C. (2007). Deep-sea ecosystem variability of the Aegean Sea during the past 22 kyr as revealed by benthic foraminifera. *Marine Micropaleontology*, *64*(3), 141–162. https://doi.org/10.1016/j.marmicro.2007.04.003

Lambeck, K., Rouby, H., Purcell, A., Sun, Y., & Sambridge, M. (2014). Sea level and global ice volumes from the Last Glacial Maximum to the Holocene. *Proceedings of the National Academy of Sciences*, *111*(43), 15296. https://doi.org/10.1073/pnas.1411762111

Langezaal, A. M., Jorissen, F. J., Braun, B., Chaillou, G., Fontanier, C., Anschutz, P., & van der Zwaan, G. J. (2006). The influence of seasonal processes on geochemical profiles and foraminiferal assemblages on the outer shelf of the Bay of Biscay. *Continental Shelf Research*, *26*(15), 1730–1755. https://doi.org/10.1016/j.csr.2006.05.005

Lascaratos, A. (1993). Estimation of deep and intermediate water mass formation rates in the Mediterranean Sea. *Deep Sea Research Part II: Topical Studies in Oceanography*, *40*(6), 1327–1332. https://doi.org/10.1016/0967-0645(93)90072-U

Lascaratos, A., Williams, R. G., & Tragou, E. (1993). A mixed-layer study of the formation of Levantine intermediate water. *Journal of Geophysical Research*, *98*(C8), 14,739–14,749. https://doi.org/doi:10.1029/93JC00912

Lea, D. W., Bijma, J., Spero, H. J., & Archer, D. (1999). Implications of a carbonate ion effect on shell carbon and oxygen isotopes for glacial ocean conditions [Inbook]. Retrieved May 2, 2019, from https://epic.awi.de/id/eprint/1921/

Lelieveld, J., Hadjinicolaou, P., Kostopoulou, E., Chenoweth, J., El Maayar, M., Giannakopoulos, C., et al. (2012). Climate change and impacts in the Eastern Mediterranean and the Middle East. *Climatic Change*, *114*(3–4), 667–687. https://doi.org/10.1007/s10584-012-0418-4

Li, L., Casado, A., Congedi, L., Dell'Aquila, A., Dubois, C., Elizalde, A., et al. (2012). 7 - Modeling of the Mediterranean climate system. In P. Lionello (Ed.), *The climate of the Mediterranean region* (pp. 419–448). Oxford: Elsevier. https://doi.org/10.1016/B978-0-12-416042-2.00007-0

Lionello, P., Malanotte-Rizzoli, P., Boscolo, R., Alpert, P., Artale, V., Li, L., et al. (2006). The Mediterranean climate: An overview of the main characteristics and issues. In P. Lionello, P. Malanotte-Rizzoli, & R. Boscolo (Eds.), *Developments in Earth and environmental sciences* (Vol. *4*, pp. 1–26). Amsterdam: Elsevier. https://doi.org/10.1016/S1571-9197(06)80003-0

Loubere, P. (2001). Nutrient and oceanographic changes in the eastern equatorial Pacific from the last full glacial to the present. *Global and Planetary Change*, *29*(1), 77–98. https://doi.org/10.1016/S0921-8181(00)00085-0

Louvari, M. A., Drinia, H., Kontakiotis, G., Di Bella, L., Antonarakou, A., & Anastasakis, G. (2019). Impact of latest-glacial to Holocene sea-level oscillations on central Aegean shelf ecosystems: A benthic foraminiferal palaeoenvironmental assessment of South Evoikos Gulf, Greece. *Journal of Marine Systems*, *199*, 103181. https://doi.org/10.1016/j.jmarsys.2019.05.007

Mackensen, A. (2008). On the use of benthic foraminiferal $d^{13}C$ in paleoceanography: Constraints from primary proxy relationships. In W. E. N. Austin & R. H. James (Eds.), *Biogeochemical controls on palaeoceanographic environmental proxies*, *Geological Society, London, Special Publications* (Vol. 303, No. 1, pp. 121–133). London: Geological Society. https://doi.org/10.1144/SP303.9

Mackensen, A., & Licari, L. (2004). Carbon isotopes of live benthic foraminifera from the South Atlantic: Sensitivity to bottom water carbonate saturation state and organic matter rain rates. In G. Wefer, S. Mulitza, & V. Ratmeyer (Eds.), *The South Atlantic in the Late Quaternary: Reconstruction of material budgets and current systems* (pp. 623–644). Berlin, Heidelberg: Springer Berlin Heidelberg. https://doi.org/10.1007/978-3-642-18917-3_27

Macklin, M. G., Toonen, W. H. J., Woodward, J. C., Williams, M. A. J., Flaux, C., Marriner, N., et al. (2015). A new model of river dynamics, hydroclimatic change and human settlement in the Nile Valley derived from meta-analysis of the Holocene fluvial archive. *Quaternary Science Reviews*, *130*, 109–123. https://doi.org/10.1016/j.quascirev.2015.09.024

Mangini, A., & Schlosser, P. (1986). The formation of Eastern Mediterranean sapropels. *Marine Geology*, *72*(1), 115–124. https://doi.org/10.1016/0025-3227(86)90102-7

Marino, G., Rohling, E. J., Sangiorgi, F., Hayes, A., Casford, J. L., Lotter, A. F., et al. (2009). Early and middle Holocene in the Aegean Sea: Interplay between high and low latitude climate variability. *Quaternary Science Reviews*, *28*(27-28), 3246–3262. https://doi.org/10.1016/j.quascirev.2009.08.011

Martín-Puertas, C., Jiménez-Espejo, F., Martínez-Ruiz, F., Nieto-Moreno, V., Rodrigo-Gámiz, M., Mata, M. d. P., & Valero-Garcés, B. (2010). Late Holocene climate variability in the southwestern Mediterranean region: An integrated marine and terrestrial geochemical approach. *Climate of the Past Discussions*, *6*(5), 1655–1683. https://doi.org/10.5194/cpd-6-1655-2010

McCorkle, D. C., Corliss, B. H., & Farnham, C. A. (1997). Vertical distributions and stable isotopic compositions of live (stained) benthic foraminifera from the North Carolina and California continental margins. *Deep Sea Research Part I: Oceanographic Research Papers*, *44*(6), 983–1024. https://doi.org/10.1016/S0967-0637(97)00004-6

McCorkle, D. C., Keigwin, L. D., Corliss, B. H., & Emerson, S. R. (1990). The influence of microhabitats on the carbon isotopic composition of deep-sea benthic foraminifera. *Paleoceanography*, *5*(2), 161–185. https://doi.org/10.1029/PA005i002p00161

McDermott, F., Mattey, D. P., & Hawkesworth, C. (2001). Centennial-scale holocene climate variability revealed by a high-resolution speleothem 18O record from SW Ireland. *Science*, *294*(5545), 1328–1331. https://doi.org/10.1126/science.1063678

McManus, J. F., Oppo, D. W., & Cullen, J. L. (1999). A 0.5-Million-Year Record of Millennial-Scale Climate Variability in the North Atlantic. *Science*, *283*(5404), 971–975. https://doi.org/10.1126/science.283.5404.971

Menna, M., & Poulain, P. M. (2010). Mediterranean intermediate circulation estimated from Argo data in 2003–2010. *Ocean Science*, *6*(1), 331–343. https://doi.org/10.5194/os-6-331-2010

Millot, C., & Taupier-Letage, I. (2005). Circulation in the Mediterranean Sea. In A. Saliot (Ed.), *The Mediterranean Sea* (pp. 29–66). Berlin, Heidelberg: Springer Berlin Heidelberg. https://doi.org/10.1007/b107143

Minto'o, C. M., Bassetti, M. A., Morigi, C., Ducassou, E., Toucanne, S., Jouet, G., & Mulder, T. (2015). Levantine intermediate water hydrodynamic and bottom water ventilation in the northern Tyrrhenian Sea over the past 56,000 years: New insights from benthic foraminifera and ostracods. *Quaternary International*, *357*, 295–313. https://doi.org/10.1016/j.quaint.2014.11.038

Mojtahid, M., Hennekam, R., De Nooijer, L. J., Reichart, G.-J., Jorissen, F., Boer, W., et al. (2019). Evaluation and application of foraminiferal element/calcium ratios: Assessing riverine fluxes and environmental conditions during sapropel S1 in the southeastern Mediterranean. *Marine Micropaleontology*, *153*, 101783. https://doi.org/10.1016/j.marmicro.2019.101783

Mojtahid, M., Jorissen, F. J., Garcia, J., Schiebel, R., Michel, E., Eynaud, F., et al. (2013). High resolution Holocene record in the south-eastern Bay of Biscay: Global versus regional climate signals. *Palaeogeography, Palaeoclimatology, Palaeoecology*, *377*, 28–44. https://doi.org/10.1016/j.palaeo.2013.03.004

Mojtahid, M., Manceau, R., Schiebel, R., Hennekam, R., & de Lange, G. J. (2015). Thirteen thousand years of southeastern Mediterranean climate variability inferred from an integrative planktic foraminiferal-based approach. *Paleoceanography*, *30*(4), 402–422. https://doi.org/doi:10.1002/2014PA002705

Moros, M., Emeis, K., Risebrobakken, B., Snowball, I., Kuijpers, A., McManus, J., & Jansen, E. (2004). Sea surface temperatures and ice rafting in the Holocene North Atlantic: Climate influences on northern Europe and Greenland. *Quaternary Science Reviews*, *23*, 2113–2126.

Murray, J. (2006). Ecology and applications of benthic foraminifera. *Palaeogeography, Palaeoclimatology, Palaeoecology*, *95*, 1–426. https://doi.org/10.1017/CBO9780511535529

Myers, P. G., Haines, K., & Rohling, E. J. (1998). Modeling the paleocirculation of the Mediterranean: The Last Glacial Maximum and the Holocene with emphasis on the formation of sapropel S1. *Paleoceanography*, *13*(6), 586–606. https://doi.org/10.1029/98PA02736

Nebout, N. C., Bout-Roumazeilles, V., Dormoy, I., & Peyron, O. (2009). Events of persistent dryness in the Mediterranean throughout the last 50 000 years. *Science et Changements Planétaires/Sécheresse*, *20*(2), 210–216. https://doi.org/10.1684/sec.2009.0181

Nicholson, S. E. (2009). A revised picture of the structure of the "monsoon" and land ITCZ over West Africa. *Climate Dynamics*, *32*(7), 1155–1171. https://doi.org/10.1007/s00382-008-0514-3

Nicholson, S. E., & Flohn, H. (1980). African environmental and climatic changes and the general atmospheric circulation in the Late Pleistocene and Holocene. *Climatic Change*, *2*(4), 313–348.

Nieto-Moreno, V., Martínez-Ruiz, F., Giralt, S., Jiménez-Espejo, F., Gallego-Torres, D., Rodrigo-Gámiz, M., et al. (2011). Tracking climate variability in the western Mediterranean during the Late Holocene: A multiproxy approach. *Climate of the Past*, *7*(4), 1395–1414. https://doi.org/10.5194/cp-7-1395-2011

Nittis, K., & Lascaratos, A. (1998). Diagnostic and prognostic numerical studies of LIW formation. *Journal of Marine Systems*, *18*, 179–195. https://doi.org/10.1016/S0924-7963(98)00011-6

Nyssen, J., Poesen, J., Moeyersons, J., Deckers, J., Haile, M., & Lang, A. (2004). Human impact on the environment in the Ethiopian and Eritrean highlands—A state of the art. *Earth-Science Reviews*, *64*(3), 273–320. https://doi.org/10.1016/S0012-8252(03)00078-3

O'Brien, S. R., Mayewski, P. A., Meeker, L. D., Meese, D. A., Twickler, M. S., & Whitlow, S. I. (1995). Complexity of Holocene climate as reconstructed from a Greenland ice core. *Science*, *270*(5244), 1962–1964. https://doi.org/10.1126/science.270.5244.1962

Ovchinnikov, I. M. (1984). The formation of intermediate water in the Mediterranean. *Oceanology*, *24*, 168–173.

Pinardi, N., & Masetti, E. (2000). Variability of the large scale general circulation of the Mediterranean Sea from observations and modelling: A review. *Palaeogeography, Palaeoclimatology, Palaeoecology*, *158*(3), 153–173. https://doi.org/10.1016/S0031-0182(00)00048-1

Peyron, O., Combourieu-Nebout, N., Brayshaw, D., Goring, S., Andrieu-Ponel, V., Desprat, S., et al. (2017). Precipitation changes in the Mediterranean basin during the Holocene from terrestrial and marine pollen records: A model-data comparison. *Climate of the Past*, *13*(3), 249–265. https://doi.org/10.5194/cp-13-249-2017

Pross, J., Kotthoff, U., Müller, U. C., Peyron, O., Dormoy, I., Schmiedl, G., et al. (2009). Massive perturbation in terrestrial ecosystems of the Eastern Mediterranean region associated with the 8.2 kyr B.P. climatic event. *Geology*, *37*(10), 887–890. https://doi.org/10.1130/G25739A.1

Raymo, M. E. (1997). The timing of major climate terminations. *Paleoceanography*, *12*(4), 577–585. https://doi.org/10.1029/97PA01169

Reiss, Z., Halicz, E., & Luz, b. (1999). Late Holocene foraminifera from the SE Levantine Basin. *Israel Journal of Earth Sciences*, *48*, 1–27.

Revel, M., Colin, C., Bernasconi, S., Combourieu-Nebout, N., Ducassou, E., Grousset, F. E., et al. (2014). 21,000 years of Ethiopian African monsoon variability recorded in sediments of the western Nile deep-sea fan. *Regional Environmental Change*, *14*(5), 1685–1696. https://doi.org/10.1007/s10113-014-0588-x

Revel, M., Ducassou, E., Skonieczny, C., Colin, C., Bastian, L., Bosch, D., et al. (2015). 20,000 years of Nile River dynamics and environmental changes in the Nile catchment area as inferred from Nile upper continental slope sediments. *Quaternary Science Reviews*, *130*, 200–221. https://doi.org/10.1016/j.quascirev.2015.10.030

Robinson, S. A., Black, S., Sellwood, B. W., & Valdes, P. J. (2006). A review of palaeoclimates and palaeoenvironments in the Levant and Eastern Mediterranean from 25,000 to 5000 years BP: Setting the environmental background for the evolution of human civilisation. *Quaternary Science Reviews*, *25*(13), 1517–1541. https://doi.org/10.1016/j.quascirev.2006.02.006

Rohling, E., Mayewski, P., Abu-Zied, R., Casford, J., & Hayes, A. (2002). Holocene atmosphere-ocean interactions: Records from Greenland and the Aegean Sea. *Climate Dynamics*, *18*(7), 587–593. https://doi.org/10.1007/s00382-001-0194-8

Rohling, E. J., Cane, T. R., Cooke, S., Sprovieri, M., Bouloubassi, I., Emeis, K. C., et al. (2002). African monsoon variability during the previous interglacial maximum. *Earth and Planetary Science Letters*, *202*(1), 61–75. https://doi.org/10.1016/S0012-821X(02)00775-6

Rohling, E. J., Hayes, A., Rijk, S. D., Kroon, D., Zachariasse, W. J., & Eisma, D. (1998). Abrupt cold spells in the northwest Mediterranean. *Paleoceanography*, *13*(4), 316–322. https://doi.org/10.1029/98PA00671

Rohling, E. J., Marino, G., & Grant, K. M. (2015). Mediterranean climate and oceanography, and the periodic development of anoxic events (sapropels). *Earth-Science Reviews*, *143*, 62–97. https://doi.org/10.1016/j.earscirev.2015.01.008

Rohling, E. J. (1994). Review and new aspects concerning the formation of eastern Mediterranean sapropels. *Marine Geology*, *122*(1), 1–28. https://doi.org/10.1016/0025-3227(94)90202-X

Rossignol-Strick, M. (1985). Mediterranean Quaternary sapropels, an immediate response of the African monsoon to variation of insolation. *Palaeogeography, Palaeoclimatology, Palaeoecology*, *49*(3), 237–263. https://doi.org/10.1016/0031-0182(85)90056-2

Rossignol-Strick, M., Nesteroff, W., Olive, P., & Vergnaud-Grazzini, C. (1982). After the deluge: Mediterranean stagnation and sapropel formation. *Nature*, *295*(5845), 105. https://doi.org/10.1038/295105a0

Scafetta, N., Milani, F., Bianchini, A., & Ortolani, S. (2016). On the astronomical origin of the Hallstatt oscillation found in radiocarbon and climate records throughout the Holocene. *Earth Science Reviews*, *162*, 24–43. https://doi.org/10.1016/j.earscirev.2016.09.004

Schilman, B., Almogi-Labin, A., & Bar-Matthews, M. (2003). Late Holocene productivity and hydrographic variability in the Eastern Mediterranean inferred from benthic foraminiferal stable isotopes. *Paleoceanography and Paleoclimatology*, *18*(3), 1064–1076. https://doi.org/10.1029/2002PA000813

Schilman, B., Almogi-Labin, A., Bar-Matthews, M., Labeyrie, L., Paterne, M., & Luz, B. (2001). Long- and short-term carbon fluctuations in the Eastern Mediterranean during the late Holocene. *Geology*, *29*, 1099–1102. https://doi.org/10.1130/0091-7613(2001)029<1099:LASTCF>2.0.CO;2

Schilman, B., Bar-Matthews, M., Almogi-Labin, A., & Luz, B. (2001). Global climate instability reflected by Eastern Mediterranean marine records during the late Holocene. *Palaeogeography, Palaeoclimatology, Palaeoecology*, *176*(1), 157–176. https://doi.org/10.1016/S0031-0182(01)00336-4

Schmiedl, G., de Bovée, F., Buscail, R., Charrière, B., Hemleben, C., Medernach, L., & Picon, P. (2000). Trophic control of benthic foraminiferal abundance and microhabitat in the bathyal Gulf of Lions, western Mediterranean Sea. *Marine Micropaleontology*, *40*(3), 167–188. https://doi.org/10.1016/S0377-8398(00)00038-4

Schmiedl, G., Kuhnt, T., Ehrmann, W., Emeis, K.-C., Hamann, Y., Kotthoff, U., et al. (2010). Climatic forcing of eastern Mediterranean deep-water formation and benthic ecosystems during the past 22 000 years. *Quaternary Science Reviews*, *29*(23-24), 3006–3020. https://doi.org/10.1016/j.quascirev.2010.07.002

Schmiedl, G., Mitschele, A., Beck, S., Emeis, K.-C., Hemleben, C., Schulz, H., et al. (2003). Benthic foraminiferal record of ecosystem variability in the eastern Mediterranean Sea during times of sapropel S5 and S6 deposition. *Palaeogeography, Palaeoclimatology, Palaeoecology*, *190*, 139–164. https://doi.org/10.1016/S0031-0182(02)00603-X

Schmiedl, G., Pfeilsticker, M., Hemleben, C., & Mackensen, A. (2004). Environmental and biological effects on the stable isotope composition of recent deep-sea benthic foraminifera from the western Mediterranean Sea. *Marine Micropaleontology*, *51*, 129–152.

Scrivner, A. E., Vance, D., & Rohling, E. J. (2004). New neodymium isotope data quantify Nile involvement in Mediterranean anoxic episodes. *Geology*, *32*(7), 565–568. https://doi.org/10.1130/G20419.1

Shanahan, T. M., McKay, N. P., Hughen, K. A., Overpeck, J. T., Otto-Bliesner, B., Heil, C. W., et al. (2015). The time-transgressive termination of the African Humid Period. *Nature Geoscience*, *8*(2), 140–144. https://doi.org/10.1038/ngeo2329

Siani, G., Magny, M., Paterne, M., Debret, M., & Fontugne, M. (2013). Paleohydrology reconstruction and Holocene climate variability in the South Adriatic Sea. *Climate of the Past*, *9*, 499–515. https://doi.org/10.5194/cp-9-499-2013

Siani, G., Paterne, M., & Colin, C. (2010). Late glacial to Holocene planktic foraminifera bioevents and climatic record in the South Adriatic Sea. *Journal of Quaternary Science*, *25*(5), 808–821. https://doi.org/10.1002/jqs.1360

Siokou-Frangou, I., Christaki, U., Mazzocchi, M. G., Montresor, M., Ribera d'Alcalá, M., Vaqué, D., & Zingone, A. (2010). Plankton in the open Mediterranean Sea: A review. *Biogeosciences*, *7*(5), 1543–1586. https://doi.org/10.5194/bg-7-1543-2010

Soon, W., Velasco Herrera, V. M., Selvaraj, K., Traversi, R., Usoskin, I., Arthur Chen, C.-T., et al. (2014). A review of Holocene solar-linked climatic variation on centennial to millennial timescales: Physical processes, interpretative frameworks and a new multiple cross-wavelet transform algorithm. *Earth Science Reviews*, *134*, 1–15. https://doi.org/10.1016/j.earscirev.2014.03.003

Spero, H. J., & Lea, D. W. (2002). The cause of carbon isotope minimum events on glacial terminations. *Science*, *296*(5567), 522–525. https://doi.org/10.1126/science.1069401

Stuiver, M., Reimer, P. J., Bard, E., Beck, J. W., Burr, G. S., Hughen, K. A., et al. (1998). INTCAL98 radiocarbon age calibration, 24,000–0 cal BP. *Radiocarbon*, *40*(3), 1041–1083. https://doi.org/10.1017/S0033822200019123

Tachikawa, K., Vidal, L., Cornuault, M., Garcia, M., Pothin, A., Sonzogni, C., et al. (2015). Eastern Mediterranean Sea circulation inferred from the conditions of S1 sapropel deposition. *Climate of the Past*, *11*(6), 855–867. https://doi.org/10.5194/cp-11-855-2015

Theodor, M., Schmiedl, G., Jorissen, F., & Mackensen, A. (2016). Stable carbon isotope gradients in benthic foraminifera as proxy for organic carbon fluxes in the Mediterranean Sea. *Biogeosciences*, *13*(23), 6385–6404. https://doi.org/10.5194/bg-13-6385-2016

Theodor, M., Schmiedl, G., & Mackensen, A. (2016). Stable isotope composition of deep-sea benthic foraminifera under contrasting trophic conditions in the western Mediterranean Sea. *Marine Micropaleontology*, *124*, 16–28.

Triantaphyllou, M. V., Ziveri, P., Gogou, A., Marino, G., Lykousis, V., Bouloubassi, I., et al. (2009). Late Glacial–Holocene climate variability at the south-eastern margin of the Aegean Sea. *Marine Geology*, *266*(1-4), 182–197. https://doi.org/10.1016/j.margeo.2009.08.005

Triantaphyllou, M. V., Gogou, A., Dimiza, M. D., Kostopoulou, S., Parinos, C., Roussakis, G., et al. (2016). Holocene climatic optimum centennial-scale paleoceanography in the NE Aegean (Mediterranean Sea). *Geo-Marine Letters*, *36*(1), 51–66. https://doi.org/10.1007/s00367-015-0426-2

Turco, M., Palazzi, E., Von Hardenberg, J., & Provenzale, A. (2015). Observed climate change hotspots. *Geophysical Research Letters*, *42*(9), 3521–3528. https://doi.org/10.1002/2015GL063891

van Helmond, N. A. G. M., Hennekam, R., Donders, T. H., Bunnik, F. P. M., de Lange, G. J., Brinkhuis, H., & Sangiorgi, F. (2015). Marine productivity leads organic matter preservation in sapropel S1: Palynological evidence from a core east of the Nile River outflow. *Quaternary Science Reviews*, *108*, 130–138. https://doi.org/10.1016/j.quascirev.2014.11.014

Weldeab, S., Emeis, K.-C., Hemleben, C., & Siebel, W. (2002). Provenance of lithogenic surface sediments and pathways of riverine suspended matter in the Eastern Mediterranean Sea: Evidence from $^{143}Nd/^{144}Nd$ and $^{87}Sr/^{86}Sr$ ratios. *Chemical Geology*, *186*(1), 139–149. https://doi.org/10.1016/S0009-2541(01)00415-6

Weldeab, S., Menke, V., & Schmiedl, G. (2014). The pace of East African monsoon evolution during the Holocene. *Geophysical Research Letters*, *41*(5), 1724–1732. https://doi.org/10.1002/2014GL059361

Woodward, J. C., Macklin, M. G., Krom, M. D., & Williams, M. A. J. (2008). The Nile: Evolution, Quaternary river environments and material fluxes. In *Large rivers*. https://doi.org/10.1002/9780470723722.ch13

Wu, J., Pahnke, K., Böning, P., Wu, L., Michard, A., & de Lange, G. J. (2019). Divergent Mediterranean seawater circulation during Holocene sapropel formation—Reconstructed using Nd isotopes in fish debris and foraminifera. *Earth and Planetary Science Letters*, *511*, 141–153. https://doi.org/10.1016/j.epsl.2019.01.036

Wüst, G. (1961). On the vertical circulation of the Mediterranean Sea. *Journal of Geophysical Research*, *66*(10), 3261–3271. https://doi.org/10.1029/JZ066i010p03261

Zeebe, R. E., Bijma, J., & Wolf-Gladrow, D. A. (1999). A diffusion-reaction model of carbon isotope fractionation in foraminifera. *Marine Chemistry*, *64*(3), 199–227. https://doi.org/10.1016/S0304-4203(98)00075-9